



**HAL**  
open science

## ”Missing links” for the long-lived Macdonald and Arago hotspots, South Pacific Ocean

L Buff, M G Jackson, K Konrad, J G Konter, M. Bizimis, A Price, Estelle F. Rose-Koga, J. Blusztajn, A. A. P. Koppers

### ► To cite this version:

L Buff, M G Jackson, K Konrad, J G Konter, M. Bizimis, et al.. ”Missing links” for the long-lived Macdonald and Arago hotspots, South Pacific Ocean. *Geology*, 2021, 49 (5), pp.541-544. 10.1130/G48276.1 . hal-03026749v2

**HAL Id: hal-03026749**

**<https://hal.science/hal-03026749v2>**

Submitted on 8 Oct 2021

**HAL** is a multi-disciplinary open access archive for the deposit and dissemination of scientific research documents, whether they are published or not. The documents may come from teaching and research institutions in France or abroad, or from public or private research centers.

L’archive ouverte pluridisciplinaire **HAL**, est destinée au dépôt et à la diffusion de documents scientifiques de niveau recherche, publiés ou non, émanant des établissements d’enseignement et de recherche français ou étrangers, des laboratoires publics ou privés.

1 “Missing links” for the long-lived Macdonald and Arago  
2 hotspots, South Pacific Ocean

3 **L. Buff<sup>1\*</sup>, M.G. Jackson<sup>1</sup>, K. Konrad<sup>2,3</sup> J.G. Konter<sup>4</sup>, M. Bizimis<sup>5</sup>, A. Price<sup>1</sup>, E.F. Rose-**  
4 **Koga<sup>6</sup>, J. Blusztajn<sup>7</sup>, A.A.P. Koppers<sup>3</sup>**

5 *<sup>1</sup>Department of Earth Science, University of California, Santa Barbara, 93106, USA*

6 *(\*corresponding author: [lbuff@ucsb.edu](mailto:lbuff@ucsb.edu))*

7 *<sup>2</sup>Department of Geoscience, University of Nevada, Las Vegas, NV 89154, USA.*

8 *<sup>3</sup>College of Earth, Ocean, and Atmospheric Sciences, Corvallis OR, 97331*

9 *<sup>4</sup>Department of Earth Sciences, University of Hawaii Manoa, Honolulu, HI 96822, USA*

10 *<sup>5</sup>School of the Earth, Ocean and Environment, University of South Carolina, Columbia, SC,*  
11 *29208, USA*

12 *<sup>6</sup>Université Clermont Auvergne, CNRS, IRD, OPGC, Laboratoire Magmas et Volcans, F-63000*  
13 *Clermont-Ferrand, France*

14 *<sup>7</sup>Department of Marine Chemistry, Woods Hole Oceanographic Institution, Woods Hole,*  
15 *Massachusetts, 02543, USA*

16  
17

18 **ABSTRACT**

19 The Cook-Austral volcanic lineament extends from Macdonald seamount (east) to Aitutaki  
20 Island (west), and comprises hotspot-related volcanic islands, seamounts, and atolls. The Cook-  
21 Australs have been characterized as multiple overlapping, age-progressive hotspot tracks  
22 generated by at least two mantle plumes, including the Arago and Macdonald plumes, which have  
23 fed volcano construction for ~20 m.y. The Arago and Macdonald hotspot tracks are argued to have

24 been active for at least 70 m.y., and to extend northwest of the Cook-Austral into the Cretaceous-  
25 aged Tuvalu-Gilbert and Tokelau Island chains, respectively. Large gaps in sampling exist along  
26 the predicted hotspot tracks, complicating efforts seeking to show that the Arago and Macdonald  
27 hotspots have been continuous, long-lived sources of hotspot volcanism back into the Cretaceous.  
28 We present new major and trace element concentrations, and radiogenic isotopes for three  
29 seamounts (Moki, Malulu, Dino) and one atoll (Rose), and new clinopyroxene  $^{40}\text{Ar}/^{39}\text{Ar}$  ages for  
30 Rose ( $24.81 \pm 1.02$  Ma) and Moki ( $44.53 \pm 10.05$  Ma). All volcanoes are located in the poorly  
31 sampled region between the younger Cook-Austral and the older, Cretaceous portions of the Arago  
32 and Macdonald hotspot tracks. Absolute plate motion modeling indicates that the Rose and Moki  
33 volcanoes lie on or near the reconstructed traces of the Arago and Macdonald hotspots,  
34 respectively, and the the  $^{40}\text{Ar}/^{39}\text{Ar}$  ages for Rose and Moki align with the predicted age progression  
35 for the Arago (Rose) and Macdonald (Moki) hotspots, thereby linking the younger Cook-Austral  
36 and older Cretaceous portions of the long-lived (>70 m.y.) Arago and Macdonald hotspot tracks.

37

## 38 INTRODUCTION

39 Intraplate volcanism is thought to result from buoyantly upwelling mantle plumes that partially  
40 melt beneath a moving plate, thereby producing age-progressive “hotspot” volcanism (e.g.,  
41 Morgan, 1971). Some plume-derived volcanic chains, such as the Hawaii-Emperor (North Pacific)  
42 and Louisville (South Pacific) chains, are well-defined with clear age progressions extending back  
43 to ~80 Ma (Sharp and Clague, 2006; O’Connor et al., 2013; Koppers et al., 2012). The Cook-  
44 Austral volcanic lineament in the South Pacific Ocean (Cook-Austral hereafter) is the  
45 manifestation of at least two overlapping hotspot tracks—the Arago (also referred to as “Rurutu”,  
46 or “Atiu trend”) and Macdonald hotspot tracks. Denser sampling may reveal that not all seamounts

47 along the predicted path of the Cook-Austral hotspots relate to these hotspots, but samples from  
48 two seamounts presented in this study strengthen hotspot age progressions anchored by young  
49 volcanism at Macdonald and Arago seamounts, respectively (Figure 1; Turner and Jarrard, 1982;  
50 Chauvel et al., 1997; Bonneville et al., 2002; Finlayson et al., 2018; Konrad et al., 2018; Rose and  
51 Koppers, 2019). While Cook-Austral volcanism has been argued to be relatively short-lived (0-20  
52 m.y.; Chauvel et al., 1997; Lassiter et al., 2003), there is growing evidence that the mantle plumes  
53 responsible for Cook-Austral volcanism are long-lived features responsible for generating Pacific  
54 seamounts during the Cretaceous (Staudigel et al., 1991; Koppers et al., 2001; 2003; 2007; Konter  
55 et al., 2008; Finlayson et al., 2018; Konrad et al., 2018).

56 Using absolute plate motion models, Koppers et al. (2003; 2007) and Konter et al. (2008)  
57 showed that Cretaceous Pacific island chains, including the Tokelau and Tuvalu-Gilbert chains,  
58 were located over the Macdonald and Arago mantle plumes, respectively (Figure 1). Konter et al.  
59 (2008) also showed geochemical similarities between the Cretaceous and Cook-Austral portions  
60 of these two hotspot tracks, strengthening the link between the younger and older segments of  
61 these hotspot tracks. Recently, Finlayson et al. (2018) and Konrad et al. (2018) showed that the  
62 Tuvalu chain captures the 50 Ma “bend” (temporally and morphologically similar to the Hawaii-  
63 Emperor Bend) of the proposed Arago hotspot, thereby strengthening the link between the younger  
64 Cook-Austral and older Cretaceous segments of this proposed long-lived hotspot. However,  
65 volcanoes sampling the 10-45 Ma portion of the Arago hotspot represent an uncharacterized gap  
66 in the hotspot track. In contrast to the Arago hotspot, the Hawaii-Emperor Bend portion of the  
67 proposed Macdonald hotspot track has not yet been identified, and it will be important for linking  
68 the more recent Cook-Austral and older Cretaceous Tokelau segments of this hotspot track. Thus,  
69 while there is growing evidence that the Macdonald and Arago hotspots have been active since at

70 least ~70 Ma, critical gaps in sampling and characterization of these two hotspot tracks weaken  
71 the hypothesis for long-lived, continuous volcanism.

72 Volcanoes in the region of the Samoan hotspot track, located ~1,000 km WNW of Aitutaki  
73 Island, were found to exhibit geochemical signatures inconsistent with nearby Samoan volcanoes  
74 (Jackson et al., 2010). Termed “interlopers” (i.e., not belonging in the region: Jackson et al. 2010),  
75 these volcanoes (Rose atoll and two seamounts, Malulu and Papatua) yielded samples exhibiting  
76 significant alteration and thick ferromanganese coatings, which contrast with the young, fresh  
77 lavas from Samoan volcanoes in the region. These interloper volcanoes also exhibit geochemical  
78 signatures consistent with an origin over Cook-Austral hotspots, which lie on, or close to, the  
79 reconstructed Macdonald and Arago hotspot traces.

80 We targeted the region between the Samoan hotspot and the Cook-Austral for additional  
81 sampling on the NOAA ocean exploration cruise EX1702 aboard the *Okeanos Explorer* in  
82 February/March 2017. Four volcanoes were sampled (Rose atoll and Malulu, Moki, and Dino  
83 seamount) by ROV (Remotely Operated Vehicle; Figure 1; Tables S1 and S2 in the  
84 Supplemental Material<sup>1</sup>). Descriptions and thin section images are publicly available for all  
85 EX1702 samples used in this study ([osu-mgr.org/noaa-ex1702](http://osu-mgr.org/noaa-ex1702)). We present new Sr-Nd-Pb-Hf  
86 isotopic data (Figures 2, S1) and major and trace element concentrations (Figure S2) on these  
87 volcanoes. The new geochemical and geochronological data, in conjunction with previously  
88 published geochemical data for two legacy samples from Rose atoll and one legacy sample each  
89 for Malulu and Papatua seamounts (obtained by deep-sea dredging; see Supplemental Materials  
90 and Jackson et al. (2010)), show that the Moki and Rose volcanoes provide “missing links”  
91 between younger Cook-Austral and older Cretaceous segments of the Macdonald and Arago

92 hotspots, respectively. These links extend the longevity of the Arago and Macdonald hotspots to  
93 at least 70 Ma, making them two of the longest-lived hotspots in the Pacific.

94

## 95 **RESULTS AND DISCUSSION**

96 Sample collection and analytical protocols for analysis of igneous material from Rose  
97 atoll and the Malulu, Moki, and Dino seamounts are detailed in the Supplemental Materials. Due  
98 to the typically high degrees of submarine alteration, fine-grained to glass-rich groundmasses  
99 and/or absence of traditionally dated phenocrystic phases (e.g. plagioclase), ages were not  
100 available for whole rock samples from these five volcanoes; nonetheless, with extensive acid  
101 leaching, we could obtain radiogenic isotopic compositions on these samples (see Supplemental  
102 Materials). However, new advancements in  $^{40}\text{Ar}/^{39}\text{Ar}$  methodology permit age determinations  
103 from clinopyroxene phenocrysts (Konrad et al., 2019). Using this technique, we successfully  
104 dated lava flows from the Moki and Rose volcanoes. The clinopyroxene separates from Rose  
105 Atoll (sample AVON2/3-D66-1) and Moki Seamount (sample EX1702-D7-2) both produced age  
106 spectrums that meet standard  $^{40}\text{Ar}/^{39}\text{Ar}$  criteria, where plateaus include  $> 60\%$  of the  $^{39}\text{Ar}_{(\text{K})}$  and  
107 probability of fit (P) values  $> 5\%$ . Two experiments for AVON2/3-D66-1, carried out on two  
108 clinopyroxene size fractions, produced concordant plateaus, which allows for the results to be  
109 combined and averaged (Figure S3). The  $^{40}\text{Ar}/^{36}\text{Ar}$  intercept values are within uncertainty of  
110 atmosphere (298.6), supporting the plateau age of  $24.81 \pm 1.02$  Ma ( $2\sigma$ ). This age places Rose  
111 atoll squarely on the age-progression for the Arago hotspot (Figure 3), which is consistent with  
112 the observation that Rose is near the reconstructed trace of the Arago hotspot (Figure 1). Sample  
113 EX1702-D7-2 contained low concentrations of potassium derived  $^{39}\text{Ar}$  and radiogenic  $^{40}\text{Ar}$ ,  
114 resulting in large uncertainties. The experiment produced a long plateau with a slightly higher-

115 than- atmospheric  $^{40}\text{Ar}/^{36}\text{Ar}$  intercept value of  $313 \pm 12$  ( $2\sigma$ ). Therefore, the inverse isochron age  
116 determination is preferred at  $44.53 \pm 10.05$  Ma ( $2\sigma$ ) (Figure S3, Tables S3,S 4). While  
117 uncertainties are large, the Moki seamount age places it on the Macdonald hotspot age  
118 progression (Figure 3).

119 New geochemical data are presented in Tables S1 and S2. In radiogenic isotopic space,  
120 Macdonald and Arago seamounts sample HIMU (high ‘ $\mu$ ’, or high  $^{238}\text{U}/^{204}\text{Pb}$ ), EM (enriched  
121 mantle) and geochemically-depleted endmembers (Chauvel and Vidal, 1992; Chauvel et al., 1997;  
122 Lassiter et al., 2003; Hanyu et al., 2013) that may reflect a contribution from a C (Common; Hanan  
123 and Graham, 1996) or FOZO (Hart et al., 1992) component (Konter et al., 2008; Figures 2, S1).  
124 While Rose atoll is erupted over the Arago hotspot, whole rock (Jackson et al., 2010) and glass  
125 geochemistry do not consistently plot in the fields for Arago hotspot volcanoes in the Cook-Austral  
126 volcanic lineament or the older portion of the Arago hotspot (Gilbert, Tuvalu, Marshall, and Wake  
127 islands and seamounts), and in some isotope spaces one or multiple Rose samples plot only in the  
128 field for Macdonald hotspot volcanoes (Figures 2, S1).

129 The Moki Seamount sample yielded an age with greater uncertainty, but the age is  
130 nonetheless consistent with a Macdonald hotspot origin, and the Moki sample consistently falls  
131 in a region of isotopic space that overlaps with Macdonald hotspot volcanoes (Figures 2, S1). In  
132 the hotspot reconstruction using the Wessel and Kroenke (2008) absolute plate motion model,  
133 Moki plots significantly closer to the reconstructed trace of the Macdonald hotspot track than the  
134 Arago hotspot track, consistent with the geochronological and geochemical data above (Figure  
135 1). While uncertainties are large, the Moki seamount age places it on the Macdonald hotspot age  
136 progression (Figure 3), and the age for Moki overlaps with the reconstructed Macdonald hotspot  
137 track, even at the  $1\sigma$  level.

138           The Dino Seamount sample and the new Malulu Seamount sample presented here  
139 (EX1702-D12-5) consistently plot in the field for Macdonald hotspot volcanoes in the Cook-  
140 Austral volcanic lineament, but age data are needed before a Macdonald hotspot designation can  
141 be assigned. Papatua seamount (Jackson et al., 2010) plots in a region that overlaps the Macdonald  
142 and Arago hotspots in all isotopic spaces for which there are available data except for the  
143  $^{206}\text{Pb}/^{204}\text{Pb}$  vs  $^{143}\text{Nd}/^{144}\text{Nd}$  isotope space where it plots in the Macdonald field (Figure 2 and Figure  
144 S1). Unfortunately, Papatua is also geographically located on a portion of the reconstructed hotspot  
145 tracks where the Macdonald and Arago tracks overlap, preventing a hotspot designation for  
146 Papatua. Age data are needed to determine the hotspot origin of this seamount.

147           The link between the younger Cook-Austral and older Cretaceous segments of the  
148 Macdonald and Arago hotspots provided by samples from Moki seamount and the Rose atoll,  
149 respectively, has two key implications: 1) it allows us to posit, with greater confidence, that the  
150 Macdonald hotspot is both continuous and long lived and 2) it supports previous arguments for the  
151 longevity of the Arago hotspot (Finlayson et al., 2018). Thus, the Macdonald and Arago hotspots  
152 join Hawaii (Tarduno et al., 2003; O'Connor et al., 2013) and Louisville (Lonsdale, 1998; Koppers  
153 et al., 2012) as two Pacific hotspots whose activity has been mapped for least 70 m.y.

154           An important outcome of this work is in strengthening the case for the longevity of the  
155 Arago and Macdonald hotspots. However, it is becoming increasingly clear that the Arago and  
156 Macdonald hotspots show significant overlap in Sr-Nd-Pb-Hf isotopic space, and it is the  
157 combination of geochemistry and ages that uniquely constrains which hotspot a given seamount  
158 belongs to. For example, the Arago and Macdonald plumes have consistently sampled the most  
159 extreme HIMU compositions ( $^{206}\text{Pb}/^{204}\text{Pb}$  up to 21.42 for Arago, and 21.93 for Macdonald;  
160 Figure 2) in the Pacific since the Cretaceous (Konter et al., 2008; Hanyu et al., 2011; Finlayson

161 et al., 2018). The reason for this may be due to the close proximity of the two hotspots: the long-  
162 lived Arago hotspot is located just ~1200 km WNW from the Macdonald hotspot. If both  
163 hotspots are fed by mantle plumes that emerge from the core-mantle boundary, the plume  
164 conduits are separated by only ~660 km at the core mantle boundary. Thus, the regions (i.e.,  
165 “feeding zones”) at the core mantle boundary that are sourcing material to the upwelling  
166 Macdonald and Arago plumes may overlap, explaining the similar isotopic signatures at both  
167 hotspots (Figure 2). If both plumes have been producing active volcanism for >70 m.y., an  
168 important dynamical question to be addressed is how the two closely-spaced plume conduits  
169 have interacted over geologic time (Lassiter et al., 2003). Both plumes arise from the large low  
170 shear-wave velocity province (LLSVP) situated on top of the core-mantle boundary beneath the  
171 Pacific (Jackson et al., 2018), and long-lived HIMU signatures in both plumes might suggest this  
172 is a geochemical characteristic of the region of the Pacific LLSVP that is sourced by both  
173 plumes.

174

175 **Acknowledgements.** We acknowledge helpful reviews from Oliver Nebel and two anonymous  
176 referees. We thank the NOAA Ocean Explorer program and crew of the *Okeanos Explorer*  
177 expedition EX1702. The Oregon State University Marine and Geology Repository provided  
178 samples from the EX1702 expedition. Konrad thanks D. Heaton for assistance with the age  
179 determinations. Jackson acknowledges support from NSF grants OCE-1912931, EAR-1900652,  
180 EAR-1429648. Rose-Koga acknowledges support from Laboratory of Excellence ClerVolc  
181 (Clermont-Ferrand Centre for Volcano Research). This is Laboratory of Excellence ClerVolc  
182 contribution number 438.

183

184 **Figure Captions**

185

186 **Figure 1. Map of the current Cook-Austral, Tokelau, and Tuvalu-Gilbert seamounts and**  
187 **volcanoes (South Pacific Ocean) pertaining to this study, showing reconstructed tracks for**  
188 **the Samoan and Cook-Austral hotspots (including Macdonald and Arago hotspots). Shaded**  
189 bands anchored to the active portions of each hotspot track are reconstructed traces for each  
190 hotspot track (dark blue=Macdonald, red=Arago, yellow=Rarotonga, purple=Samoa), and are  
191 based on the Wessel and Kroenke (2008) absolute plate motion model; stars mark proposed  
192 hotspot locations. Blue circles represent volcanoes previously associated with the Macdonald  
193 hotspot and red circles represent volcanoes previously associated with the Arago hotspot (data  
194 sources are from the following: Koppers et al., 2007; Konrad et al., 2018; Rose and Koppers,  
195 2019; Jackson et al., 2020). The five interloper volcanoes investigated in this study—Moki,  
196 Malulu, Rose, Dino, and Papatua—are also indicated in the map.

197

198 **Figure 2.  $^{143}\text{Nd}/^{144}\text{Nd}$  versus  $^{206}\text{Pb}/^{204}\text{Pb}$  for volcanoes in this study plotted with existing data**  
199 **from Macdonald and Arago hotspot-related volcanoes.** The Moki and Malulu isotopic data  
200 produced for this study are from clinopyroxene phenocrysts, as seawater alteration prevented the  
201 analysis of whole rock samples. New data also include pillow rim glass analyses from Rose atoll,  
202 whole rock data from Dino seamount, and previously-published whole rock data on Rose, Malulu,  
203 and Papatua lavas from Jackson et al. (2010). The younger portions of the Arago (red field) and  
204 Macdonald (blue) hotspots in the Cook-Austral volcanic lineament are distinguished from the  
205 older portions of these hotspots (light grey with long dashed lines for the Tuvalu, Gilbert, Marshall  
206 and Wake islands and seamounts [i.e., Old Arago]; dark grey with short dashed lines for the

207 Tokelau Islands and seamounts [i.e., Old Macdonald]). Age-corrected (to the time of eruption)  
208 isotopic values are shown, but only where ages are available (Moki, and Rose atoll). The three  
209 undated Rose samples are assumed to have the same age as sample EX1702-D3-2. The isotopic  
210 shift due to the age correction is shown by the line extending from the respective datapoints (which  
211 represents the magnitude and direction of the age correction). The other samples (Malulu, Papatua,  
212 and Dino) are not associated with ages and age corrections are not provided. All data not produced  
213 in this study was previously published and downloaded from the Georoc database  
214 (<http://georoc.mpch681mainz.gwdg.de/georoc>). HIMU—high  $\mu$  = high  $^{238}\text{U}/^{204}\text{Pb}$ ; EM1-EM2—  
215 enriched mantle sources. Figure is modified after Jackson et al. (2020).

216

217 **Figure 3. Hotspot track age-distance plot showing Rose and Moki volcanoes (South Pacific**  
218 **Ocean), including volcanoes associated with the Macdonald, Arago, Rarotonga, and Samoa**  
219 **trends plotted along their respective reconstructed hotspot track.** The clinopyroxene  
220 incremental heating  $^{40}\text{Ar}/^{39}\text{Ar}$  ages for Rose and Moki are labeled (and shown with  $2\sigma$   
221 uncertainties). Great circle distances from the active hotspots are used. The Wessel and Kroenke  
222 (2008) absolute plate motion model, used to model volcanic age progressions, is shown for each  
223 hotspot (blue=Macdonald, red=Arago, black=Rarotonga, and pink=Samoa). Estimates for the  
224 uncertainty in the Wessel and Kroenke (2008) model are also provided (dashed lines). Ages for  
225 the Tokelau and Tuvalu-Gilbert volcanoes were published by Staudigel et al. (1991), Koppers et  
226 al. (2003) Konter et al. (2008), Finlayson et al. (2018), and Konrad et al. (2018). Ages for the  
227 Cook-Austral volcanic lineament are compiled in Jackson et al. (2020) and Rose and Koppers  
228 (2019).

229

230 <sup>1</sup>Supplemental Material. Methodology for the sample analyses, data tables for the radiogenic  
231 isotopes, major and trace elements, and successful <sup>40</sup>Ar/<sup>39</sup>Ar dates, and additional figures provided  
232 here. Please visit <https://doi.org/10.1130/XXXXX> to access the supplemental material, and contact  
233 editing @geosociety.org with any questions.

234

235

### 236 **References Cited**

237 Bonneville, A., Le Suave, R., Audin, L., Clouard, V., Dosso, L., Gillot., P.Y., Janney, P., and  
238 Maamaatuaiahutapu, K., 2002, Arago Seamount: The missing hotspot found in the  
239 Austral Islands. *Geology*, v. 30, p. 1023-1026.

240

241 Chauvel, C., McDonough, W., Guille, G., Maury, R., and Duncan, R., 1997, Contrasting old and  
242 young volcanism in Rurutu Island, Austral chain. *Chemical Geology*, v. 139, p. 125-143.

243

244 Chauvel, C., Hofmann, A.W., and Vidal, P., 1992, HIMU-EM: the French Polynesian  
245 connection. *Earth and Planetary Science Letters*, v. 110, p. 99–119.

246

247 Finlayson, V., Konter, J.G., Konrad, K., Koppers, A.A.P., Jackson, M.G., and Rooney, T.O.,  
248 2018, Sr–Pb–Nd–Hf isotopes and <sup>40</sup>Ar/<sup>39</sup>Ar ages reveal a Hawaii–Emperor-style bend in  
249 the Rurutu hotspot. *Earth and Planetary Science Letters*, v. 500, p. 168–179.

250

251 Hanan, B. B., Graham, W. D., 1996, Lead and Helium Isotope Evidence from Oceanic Basalts

252 for a Common Deep Source of Mantle Plumes. *Science*, v. 272, p. 991-995, doi:  
253 10.1126/science.272.5264.991.  
254  
255 Hanyu, T., Tatsumi, Y., Senda, R., Miyazaki, T., Chang, Q., Hirahara, Y., Takahashi, T.,  
256 Kawabata, H., Suzuki, K., Kimura, J., Nakai, S., 2011, Geochemical characteristics and  
257 origin of the HIMU reservoir: A possible mantle plume source in the lower mantle.  
258 *Geochemistry, Geophysics, Geosystems*, v. 12, Q0AC09.  
259  
260 Hanyu, T., Dosso, L., Ishizuka, O., Tani, K., Hanan, B.B., Adam, C., Nakai, S., Senda, R.,  
261 Chang, Q., and Tatsumi, Y., 2013, Geochemical diversity in submarine HIMU basalts  
262 from Austral Islands, French Polynesia. *Contributions to Mineralogy and Petrology*, v.  
263 166, p. 1285–1304.  
264  
265 Hart, S. R., Hauri, E. H., Oschmann, L. A., Whitehead, J. A., 1992, Mantle Plumes and  
266 Entrainment: Isotopic Evidence. *Science*, v. 256, p. 517-520, doi:  
267 10.1126/science.256.5056.517.  
268  
269 Jackson, M.G., Hart, S.R., Konter, J.G., Koppers, A.A.P., Staudigel, H., Kurz, M.D., Blusztajn,  
270 J., and Sinton, J.M., 2010, The Samoan hotspot track on a “hotspot highway”:  
271 Implications for mantle plumes and a deep Samoan mantle source. *Geochemistry,*  
272 *Geophysics, Geosystems*, v. 11, Q12009, doi:10.1029/2010GC003232.  
273  
274 Jackson, M.G., Becker, T.W., Konter, J.G., 2018, Geochemistry and distribution of recycled

275 domains in the mantle inferred from Nd and Pb isotopes in oceanic hot spots:  
276 implications for storage in the large low shear wave velocity provinces. *Geochemistry,*  
277 *Geophysics, Geosystems*, v. 19, p. 3496-3519.

278

279 Jackson, M.G., Halldórsson, S.A., Price, A., Kurz, M.D., Konter, J.G., Koppers, A.A.P., Day,  
280 J.M.D., 2020, Contrasting old and young volcanism from Aitutaki, Cook Islands:  
281 Implications for the origins of the Cook-Austral volcanic chain. *Journal of Petrology*,  
282 egaa037, <https://doi.org/10.1093/petrology/egaa037>.

283

284 Konrad, K., Koppers, A.A.P., Steinberger, B., Finlayson, V., Konter, J., and Jackson, M.G.,  
285 2018, On the relative motions of long-lived Pacific mantle plumes. *Nature*  
286 *Communications*, v. 9, 854, DOI: 10.1038/s41467-018-03277-x.

287

288 Konrad, K., Koppers, A. A., Balbas, A. M., Miggins, D. P., & Heaton, D. E., 2019. Dating  
289 clinopyroxene phenocrysts in submarine basalts using  $^{40}\text{Ar}/^{39}\text{Ar}$  geochronology.  
290 *Geochemistry, Geophysics, Geosystems*, v. 20, p. 1041-1053.

291

292 Konter, J.G., Hanan, B.B., Blichert-Toft, J., Koppers, A.A.P., Plank, T., Staudigel, H., 2008, One  
293 hundred million years of mantle geochemical history suggest the retiring of mantle  
294 plumes is premature. *Earth and Planetary Science Letters*, v. 275, p. 285-295.

295

296 Koppers, A.A.P., Phipps Morgan, J., and Staudigel, H., 2001, Testing the fixed hotspot

297 hypothesis using  $^{40}\text{Ar}/^{39}\text{Ar}$  age progressions along seamount trails. *Earth and Planetary*  
298 *Science Letters*, v. 185, p. 237-252.

299

300 Koppers, A.A.P., Pringle, M.S., Wijbrans, J.R., 2003, Short-lived and discontinuous intraplate  
301 volcanism in the South Pacific: Hot spots or extensional volcanism? *Geochemistry,*  
302 *Geophysics, Geosystems*, v. 4, 1089.

303

304 Koppers, A.A.P., Staudigel, H., Phipps Morgan, J., and Duncan, R.A., 2007, Nonlinear  
305  $^{40}\text{Ar}/^{39}\text{Ar}$  age systematics along the Gilbert Ridge and Tokelau Seamount Trail and the  
306 timing of the Hawaii-Emperor Bend. *Geochemistry, Geophysics, Geosystems*, v. 8,  
307 Q06L13, doi:10.1029/2006GC001489.

308

309 Koppers, A.A.P., Yamazaki, T., Geldmacher, J., Gee, J.S., Pressling, N., Hoshi, H., Anderson,  
310 L., Beier, C., Buchs, D.M., Chen, L.-H., Cohen, B.E., Deschamps, F., Dorais, M.J.,  
311 Ebuna, D., Ehmann, S., Fitton, J.G., Fulton, P.M., Ganbat, E., Hamelin, C., Hanyu, T.,  
312 Kalnis, L., Kell, J., Machida, S., Mahoney, J.J., Moriya, K., Nichols, A.R.L., Rausch, S.,  
313 Sano, S., Sylvain, J.B., and Williams, R., 2012, Limited latitudinal mantle plume motion  
314 for the Louisville hotspot. *Nature Geoscience*, v. 5, p. 911–917.

315

316 Lassiter, J.C., Blichert-Toft, J., Hauri, E.H., Barszczus, H.G., 2003, Isotope and trace element  
317 variations in lavas from Raivavae and Rapa, Cook–Austral islands: constraints on the  
318 nature of HIMU- and EM-mantle and the origin of mid-plate volcanism in French  
319 Polynesia. *Chemical Geology*, v. 202, p. 115–138.

320

321 Lonsdale, P., 1988, Geography and history of the Louisville hotspot chain in the southwest  
322 Pacific. *Journal of Geophysical Research*, v. 93, p. 3078-3104.

323

324 Morgan, W.J., 1971, Convection Plumes in the Lower Mantle. *Nature*, v. 230, p. 42-43.

325

326 O'Connor, J.M., Steinberger, B., Regelous, M., Koppers, A.A.P., Wijbrans, J.R., Haase, K.M.,  
327 Stoffers, P., Jokat, W., and Garbe-Schönberg, D., 2013, Constraints on past plate and  
328 mantle motion from new ages for the Hawaiian-Emperor Seamount Chain. *Geochemistry,*  
329 *Geophysics, Geosystems*, v. 20, p. 4756-4778. <https://doi.org/10.1029/2019GC008302>.

330

331 Rose, J., and Koppers, A.A.P., 2019, Simplifying age progressions within the Cook-Austral  
332 Islands using high-resolution ARGUS-VI  $^{40}\text{Ar}/^{39}\text{Ar}$  incremental heating ages.  
333 *Geochemistry, Geophysics, Geosystems*, v. 14, p. 4564-4584.

334

335 Sharp, W.D., and Clague, D.A., 2006, 50-Ma initiation of Hawaiian-Emperor bend records major  
336 change in Pacific plate motion. *Science*, v. 313, p. 1281-1284.

337

338 Staudigel, H., Park, K.-H., Pringle, M., Rubenstone, J.L., Smith, W.H.F., and Zindler, A., 1991,  
339 The longevity of the South Pacific isotopic and thermal anomaly. *Earth and Planetary*  
340 *Science Letters*, v. 102, p. 24-44.

341

342 Tarduno, J.A., Duncan, R.A., Scholl, D.W., Cottrell, R.D., Steinberger, B., Thordarson, T., Kerr,

343 B.C., Neal, C.R., Frey, F.A., Torii, M., and Carvallo, C., 2003, The Emperor Seamounts:  
344 Southward motion of the Hawaiian hotspot plume in Earth's mantle. *Science*, v. 301, p.  
345 1064-1069.

346

347 Turner, D.L., and Jarrard, R.D., 1982. K/Ar dating of the Cook Austral island chain; a test of the  
348 hot spot hypothesis. *Journal of Volcanology and Geothermal Research*, v. 12, p. 187–  
349 220.

350

351 Wessel, P., and Kroenke, L.W., 2008, Pacific absolute plate motion since 145Ma: an assessment  
352 of the fixed hot spot hypothesis. *Journal of Geophysical Research*, v.113, B06101.  
353 <https://doi.org/10.1029/2007JB005499>.

354

355

356

## 357 Supplemental Materials

358

### 359 **Methods**

360 *Sample locations, preparation and wet chemistry.*

361 The samples in this study were collected by deep submarine dredging from four  
362 seamounts (Papatua, Moki, Seamount D [“Dino”], Malulu) and one atoll (Rose) in the Samoan  
363 region. Several samples in this study were collected during the 2017 expedition (EX1702) aboard  
364 the NOAA *Okeanos Explorer*: Moki seamount (basaltic sample D7-2), Dino seamount (basaltic  
365 sample D11-1), Rose atoll (pillow fragment sample D3-2), and Malulu seamount (hyaloclastite  
366 sample D12-5). Finally, two samples from the 1999 AVON2/3 expedition aboard the R/V  
367 Melville which were previously characterized are presented here with modern Pb-isotopic  
368 analyses: AVON2/3-D67-11 from Malulu seamount which is an altered basalt, and basaltic  
369 sample AVON2/3-D66-1 from Rose atoll. Tables S1 and S2 present previously published data on  
370 these two Rose samples in addition to two other samples—AVON2/3-D65-18 (from Malulu  
371 seamount) and ALIA-DR129-05 (from Papatua seamount) —from non-Samoan seamounts in the  
372 Samoan region. Sample locations and geochemical characterization of these four previously  
373 published lavas can be found in **Jackson et al. (2010)**.

374 Samples were crushed in plastic bags to avoid exposure to metal. Crushed material was  
375 then sieved. For two samples (EX1702-D12-5 hyaloclastite from Malulu seamount and EX1702-  
376 D7-2 basalt from Moki seamount), clinopyroxene was removed for radiogenic isotopic work due  
377 to the lack of fresh basaltic material. For Rose atoll sample EX1702-D3-2, volcanic glass was  
378 removed from the pillow rim for radiogenic isotopic analysis (this glass was also characterized  
379 for major and trace element compositions, but we also present whole rock major and trace  
380 element data for this sample as well). For sample EX1702-11-1 (Seamount D), 200 mg of the  
381 freshest (0.5 to 1 mm) rock chips were analyzed, targeting groundmass. We also separated the  
382 freshest groundmass chips from two previously characterized lavas—AVON2/3-D66-1 (Rose  
383 atoll) and AVON2/3-D67-11 (Malulu seamount)—for a new characterization using modern Pb  
384 isotopic analyses and new analyses of Sr and Nd isotopes on the same material.

385 The groundmass samples (including the EX1702-D3-2 glass) were treated with a heavy  
386 leaching protocol described in **Price et al. (2016)** which, in addition to the 6N HCl leaching  
387 treatment, uses hot 4N HNO<sub>3</sub> and hot 30% H<sub>2</sub>O<sub>2</sub>. The clinopyroxene samples were first leached  
388 in concentrated HCl for 1 hour at 40° C, then in concentrated nitric for 1 hour at 40° C, with ~1  
389 hour of sonication in the same acid following each leaching step; after this initial leach, the  
390 clinopyroxenes were subjected to the same “heavy leaching” as the groundmass and glass  
391 samples (and, following leaching, only pristine clinopyroxenes were selected for dissolution and  
392 analysis). Note that replicated analysis of the D11-1 groundmass followed additional leaching: it  
393 was treated with the strong leaching protocol followed by an additional 8 hours of leaching in 6N  
394 HCl at 60° C and an additional 10 minutes leaching in cold concentrated HF; this may explain  
395 the offset in Sr, Nd, and Pb isotopes between the original and replicate rounds of analyses of this  
396 sample. USGS reference materials were not leached. Following leaching, samples were rinsed  
397 and sonicated repeatedly in MilliQ H<sub>2</sub>O ( $\geq 18.2$  M $\Omega \cdot$  cm deionized water). Sample dissolution,  
398 wet chemistry (including Sr, Pb, Hf and Nd elemental separations), and mass spectrometry was  
399 carried out in one of the three following institutions:

- 400 1. One batch of samples underwent Sr, Nd, and Pb chemical separations at UCSB, with Sr  
401 and Nd isotopes analyzed on the UCSB TIMS and Pb isotopes analyzed on the WHOI

402 MC-ICP-MS; the wet chemistry follows methods developed in **Price et al. (2014)** with  
403 modifications as follows: Following dissolution in concentrated HF and HNO<sub>3</sub>, Sr and Pb  
404 were purified by two passes through 100 µL of Eichrom Sr resin (25-50 µm), and Nd  
405 purified was purified from the wash of the Sr resin using a two-step method employing  
406 Eichrom TRU resin (100-150 µm) followed by Eichrom LN-Spec resin (50-100 µm).  
407 Total procedural blanks are <200 pg for Sr, <50 pg for Nd, and < 120 pg for Pb.

- 408 2. A second batch of samples underwent Sr, Nd, and Pb chemical separations at UCSB as  
409 described above, with Sr and Nd isotopes analyzed on the UCSB TIMS. However, Pb  
410 isotopes were analyzed on the University of South Carolina MC-ICP-MS.
- 411 3. A third batch of samples, which included just the cpx separates for EX1702-D12-5 and  
412 EX1702-D7-5, underwent dissolution, chemical separations (for Sr, Nd, Hf, and Pb), and  
413 mass spectrometry at the University of South Carolina.

414 Further description of wet chemistry and mass spectrometry is provided below.

415

416 *Sr and Nd mass spectrometry at UCSB and Pb mass spectrometry at WHOI.*

417 Sr and Nd isotopes were analyzed on a Thermo Triton Plus TIMS mass spectrometer  
418 housed at UCSB. 500 ng of Sr or Nd was loaded on outgassed, zone-refined Re (99.999% purity,  
419 H-Cross, USA) filaments. With the exception of the first <sup>87</sup>Sr/<sup>86</sup>Sr analyses (EX1702-D12-5  
420 clinopyroxene, EX1702-D7-5 clinopyroxene, EX1702-D11-1, EX1702-D3-2) and associated  
421 standards, which used a 33 picoamp gainboard but did not employ amplifier rotation, all other Sr  
422 and Nd isotopic analyses of samples, replicates, and associated standards employed amplifier  
423 rotation on 10<sup>11</sup> ohm amplifiers and a 3.3 picoamp gainboard. Gains were run with the start of a  
424 new barrel. Approximately 20% of analysis time was devoted to baselines: baselines are taken  
425 with each rotation of the amplifiers (i.e., because 5 amplifiers-cup pairs were used during  
426 analyses, 5 baselines were taken during each full amplifier rotation). Intensities were kept at  
427 approximately 3V on mass 88 and 3V on mass 144 during <sup>87</sup>Sr/<sup>86</sup>Sr and <sup>143</sup>Nd/<sup>144</sup>Nd analyses,  
428 respectively. Sr and Nd isotopes were corrected for mass bias assuming an exponential law and  
429 using canonical <sup>86</sup>Sr/<sup>88</sup>Sr and <sup>146</sup>Nd/<sup>144</sup>Nd ratios of 0.1194 and 0.7219, respectively. Isobaric  
430 interferences from Rb and Sm were corrected by monitoring masses 85 and 147, but corrections  
431 to the <sup>87</sup>Sr/<sup>86</sup>Sr and <sup>143</sup>Nd/<sup>144</sup>Nd ratios were nominal. USGS reference materials (processed  
432 through all steps of wet chemistry and column chemistry with unknowns at UCSB) and sample  
433 unknowns were corrected for the offset between preferred and measured standard (NBS987 or  
434 JNdi) values with each barrel: preferred value for NBS987 <sup>87</sup>Sr/<sup>86</sup>Sr is 0.710240, and JNdi is  
435 0.512099 (**Garçon et al., 2018**). On the UCSB Triton Plus the average <sup>87</sup>Sr/<sup>86</sup>Sr and <sup>143</sup>Nd/<sup>144</sup>Nd  
436 and long-term reproducibility, up to and including this study, of NBS987 and JNdi using  
437 amplifier rotation is 0.710246 ± 0.000011 (2SD, N=29) and, 0.512100 ± 0.000004 (2SD, N=27),  
438 respectively. The corresponding average <sup>87</sup>Sr/<sup>86</sup>Sr and long-term reproducibility when analyzing  
439 NBS987 without amplifier rotation is 0.710244 ± 0.000014 (2SD, N=39).

440 We note that prior analyses of the AVON2/3 cruise samples from Rose (AVON2/3-66-1)  
441 and Malulu (AVON2/3-67-11), reported in **Jackson et al. (2010)**, should be replaced by new  
442 analyses of these two samples shown in **Table S1**, for two reasons: 1) the previously published  
443 Pb isotopic analyses were made by TIMS without a spike addition to control for in-run mass  
444 fractionation and 2) these two samples exhibit significant alteration and acid leaching for the  
445 prior analyses may not have been sufficient to have removed alteration phases. We note that the  
446 new <sup>143</sup>Nd/<sup>144</sup>Nd analysis for AVON2/3-67-11 (0.512982) shows significant disagreement with  
447 the prior analysis (0.512796, after correction to the JNdi reference frame use here by applying

448 the La Jolla to JNdi conversion from **Tanaka et al., 2000**) made at WHOI in the year 2000 and  
449 reported by **Jackson et al. (2010)**. In order to evaluate the accuracy of the new  $^{143}\text{Nd}/^{144}\text{Nd}$   
450 measurement, three additional aliquots of this sample were obtained from the WHOI dredge  
451 repository, including the original bag of crushed rock chips for this sample from which material  
452 was extracted for the 2000 analysis (see AVON2/3-67-11 rep1, rep2, and rep3 in **Table S1**); new  
453 batches of chips were prepared by separately crushing each aliquot, and the different aliquots of  
454 chips were leached and underwent wet chemistry and mass spectrometry during a separate  
455 session than the original analyses. The three replicate  $^{143}\text{Nd}/^{144}\text{Nd}$  analyses (0.512982, 0.512980,  
456 and 0.512981) show excellent agreement with the new  $^{143}\text{Nd}/^{144}\text{Nd}$  result, confirming its  
457 accuracy. We note that the new analyses of Sr and Pb isotopes for this sample are similar to the  
458 published data for this sample reported in **Jackson et al. (2010)**.

459 Using the Pb fractions purified at UCSB, Pb isotopic analyses were carried out at the  
460 Woods Hole Oceanographic Institution using the Thermo Neptune MC-ICP-MS housed there  
461 (**Hart and Blusztajn, 2006**). Fractionation correction was made by Tl-addition assuming an  
462 exponential fractionation law (**White et al., 2001**). Samples and an aliquot of AGV-2 (processed  
463 through all steps of column chemistry and mass spectrometry with the samples) were corrected  
464 for the offset between preferred (i.e., values from **Eisele et al., 2003**) and measured ratios of  
465 NBS981.

466 For a different subset of samples (specified in **Table S2**), Pb fractions purified at UCSB  
467 were carried out at the University of South Carolina on Thermo Neptune MC-ICP-MS housed  
468 there. The samples, together with an aliquot of BCR-2 (processed through all steps of column  
469 chemistry and mass spectrometry with the samples) were corrected for the offset between  
470 preferred (i.e., values from **Eisele et al., 2003**) and measured ratios of NBS981.

471  
472 *Sr, Nd, Hf and Pb isotopic and major and trace element concentrations on clinopyroxenes from*  
473 *samples EX1702-D12-5 and EX1702-D7-5 at U. South Carolina.*

474 Following leaching, visually fresh clinopyroxenes were picked under a binocular  
475 microscope. The clinopyroxene samples were then processed at the Center for Elemental Mass  
476 Spectrometry, University of South Carolina. Approximately 150-200 mg of sample was first  
477 leached (using the same protocol described above) and dissolved in Teflon distilled HF:HNO<sub>3</sub>  
478 (3:1) mixture on a hot plate for ~ 3 days, with frequent sonication. After drydown the samples  
479 were picked in 6N HCl with added boric acid in 10N HCl to complex fluorides, which increases  
480 yields in Hf chemistry (**Frisby et al., 2016**). Afterwards the samples were converted to nitrates.  
481 A small aliquot (~5%) was taken for Sr and Nd isotopes and the remainder was dried down with  
482 HBr for Pb and then Hf chemistry. A precisely determined aliquot of the dissolved  
483 clinopyroxene samples was pipetted from the solution and gravimetrically diluted for trace  
484 element analyses prior to the splitting of Sr-Nd and Pb-Hf fractions. Trace elements were then  
485 analyzed by ICP-MS with an aliquot of BHVO-1 on the Element2 following established methods  
486 for the lab (e.g. **Frisby et al, 2016**).

487 For the chemical separations, Sr was separated first on an Eichrom Sr-spec resin and the  
488 washes containing the rest of the elements were processed through an Eichrom TRU spec resin  
489 to concentrate the LREEs, and then on an Eichrom Ln-Resin to isolate Nd (**Frisby et al, 2016**).  
490 The Pb was separated on anion resin in HBr and HCl media, and the washes from that were  
491 processed for Hf following the method of **Munker et al. (2001)**. An unleached BCR-2 powder  
492 was dissolved and processed through all steps of chemistry and mass spectrometry with sample  
493 unknowns. Total procedural blanks during the analytical session were 10 pg for Pb, 180 pg for

494 Sr, <10 pg for Nd, and 40 pg for Hf.

495 The isotopic compositions of Sr, Nd, Pb, and Hf were measured on the Thermo Neptune  
496 housed at the University of South Carolina following methods provided in **Beguelin et al.,**  
497 **(2017)**. All samples were corrected for mass bias using the exponential law: Pb was corrected  
498 using the Tl addition method (**White et al., 2001**),  $^{87}\text{Sr}/^{86}\text{Sr}$  was corrected using  $^{86}\text{Sr}/^{88}\text{Sr}$  of  
499 0.1194,  $^{143}\text{Nd}/^{144}\text{Nd}$  was corrected using  $^{146}\text{Nd}/^{144}\text{Nd}$  of 0.7219, and  $^{176}\text{Hf}/^{177}\text{Hf}$  was corrected  
500 using  $^{179}\text{Hf}/^{177}\text{Hf}$  of 0.7325. All isotopic data on samples were corrected for the offset between  
501 measured and preferred standards using the following preferred values: SRM981 values from  
502 **Eisele et al. (2003)** ( $^{206}\text{Pb}/^{204}\text{Pb} = 16.9409$ ,  $^{207}\text{Pb}/^{204}\text{Pb} = 15.4976$ , and  $^{208}\text{Pb}/^{204}\text{Pb} = 36.7262$ );  
503 NBS987  $^{87}\text{Sr}/^{86}\text{Sr}$  value of 0.710240; JMC-475  $^{176}\text{Hf}/^{177}\text{Hf}$  value of 0.282160; JNdi  $^{143}\text{Nd}/^{144}\text{Nd}$   
504 value of 0.512099 (**Garçon et al., 2018**).

505 During the course of these measurements, reproducibility of  $^{87}\text{Sr}/^{86}\text{Sr}$  on NBS987 was 22  
506 ppm, of  $^{143}\text{Nd}/^{144}\text{Nd}$  on JNdi-1 was 20 ppm, of  $^{176}\text{Hf}/^{177}\text{Hf}$  on JMC-475 was 28 ppm, and Pb  
507 isotopic compositions on NBS981 were 62ppm on  $^{206}\text{Pb}/^{204}\text{Pb}$ , 68 ppm for  $^{207}\text{Pb}/^{204}\text{Pb}$ , and 80  
508 ppm for  $^{208}\text{Pb}/^{204}\text{Pb}$  (all 2SE). An unleached BCR-2 powder was run together with the  
509 clinopyroxenes through all steps of column chemistry and mass spectrometry, and data are  
510 shown in **Table S1**.

511

512 *Whole rock major and trace element analyses at Washington State University.*

513 For samples EX1702-D7-2, EX1702-D3-2, and EX1702-D11-1, 10 to 20 g blocks of rock  
514 were cut with the rock saw, and care was taken to avoid visibly altered portions of rock. The  
515 blocks were cleaned with silicon carbide sand paper, and sonicated in MilliQ H<sub>2</sub>O. Samples were  
516 crushed and then powdered in an agate shatterbox (with cleaning with silica between barrels) at  
517 the Geoanalytical lab at the Washington State University (WSU). Major and trace element  
518 concentrations were obtained at WSU by X-ray fluorescence (XRF) and ICP-MS. XRF and ICP-  
519 MS methods, and evaluation of accuracy using international standards, are reported elsewhere  
520 (**Knaack et al., 1994; Johnson et al., 1999**), but summarized briefly here. The precision ( $1\sigma$ ) for  
521 major elements in basalts by XRF is 0.11–0.33% ( $1\sigma$ ) of the amount present for SiO<sub>2</sub>, Al<sub>2</sub>O<sub>3</sub>,  
522 TiO<sub>2</sub>, P<sub>2</sub>O<sub>5</sub>) and 0.38–0.71% for other elements. Trace element precision of basalts by ICP-MS is  
523 0.77–3.2% ( $1\sigma$ ) for trace elements except for U (9.3%) and Th (9.5%). An aliquot of the USGS  
524 reference material BCR-2 was analyzed as an unknown together with the basaltic unknowns, and  
525 the data are reported in **Table S2**. The new analysis of BCR-2 reported here is compared major  
526 and trace element compositions for this reference material reported in **Jochum et al. (2016)**.  
527 Whole rock major and trace element analyses of the AVON2/3-67-1, AVON2/3-66-1,  
528 AVON2/3-65-18 and ALIA-DR129-05 were made following the same methods and data are  
529 reported in **Jackson et al. (2010)**.

530

531 *In situ major element analyses on glass by electron microprobe at UC Santa Barbara.*

532 Glass was available for EX1702-D3-2. Sample chips were analyzed by electron  
533 microprobe at UC Santa Barbara using primary standards and following analytical conditions  
534 outlined in **Jackson et al. (2015)**. The MORB basaltic secondary standard 519-4-1 was analyzed  
535 repeatedly throughout the analytical session. Major element compositions for sample unknown  
536 glass and the secondary standard (and previously published data on this secondary standard from  
537 **Melson et al., 2002**) are reported in **Table S2**.

538

539 *In situ trace element analyses by LA-ICP-MS at Clermont-Ferrand.*

540 Trace element analyzes on the EX1702-D3-2 glass sample were made using a laser  
541 ablation ICP-MS system housed at Laboratoire Magmas et Volcans at Clermont-Ferrand.  
542 Analytical methods are outlined in **Oulton et al. (2016)** and **Reinhart et al. (2018)**. Analyses  
543 were made using a Thermo Scientific Element XR ICP-MS coupled to a Resonetics M-50E 193  
544 nm ArF excimer laser.  $^{43}\text{Ca}$  was used as an internal standard. All surfaces were preablated (for 1s  
545 at 10Hz) prior to analysis. Analyses of samples and standards used a 47  $\mu\text{m}$  laser spot, and the  
546 laser was fired with a 4 Hz repetition rate. Analyses were conducted over 80 second ablation  
547 periods, with 20 seconds of blank analysis (with the laser off) before samples analysis and  
548 (following a washout period) 20 seconds of blank analysis (again, with the laser off) after the  
549 analysis. Analyses were made in low resolution mode using triple mode with a 20% mass  
550 window and a 20 ms integration window. Acceleration voltage was scanned between magnet  
551 scans to ensure peak positions were maintained. Calibration curves were generated using  
552 NIST612 (**Gagnon et al., 2008**) and BCR-2 (**Jochum et al., 2006**) glass. Replicate analyses of a  
553 MORB glass, 519-4-1, were made throughout the analytical session to monitor precision and  
554 accuracy of analyses. The reproducibility of the trace element analyses was better than 10%  
555 (2RSD, N=8) for all elements except for Cs (44%). Measured concentrations are compared with  
556 previously published analyses from **Gale et al. (2013)** in **Table S2**.

557

## 558 **Figure Captions**

559

560 **Figure S1. Isotopic data for volcanoes in this study plotted with existing data for Macdonald**  
561 **and Arago volcanoes.** The Rose atoll, Malulu seamount, and Dino seamount are all  
562 geochemically linked to the Macdonald hotspot, consistently grouping with Macdonald-type  
563 volcanoes. The Moki seamount falls into the region where the Macdonald and Arago isotope  
564 spaces overlap in all plots except for the plot of  $^{176}\text{Hf}/^{177}\text{Hf}$  versus  $^{143}\text{Nd}/^{144}\text{Nd}$  where it clearly  
565 links to Macdonald. A hotspot origin for Papatua cannot be determined as it consistently plots in  
566 the region of overlap between Macdonald and Arago isotope spaces. The Moki and Malulu isotopic  
567 data produced for this study are from clinopyroxene phenocrysts, as seawater alteration prevented  
568 the analysis of whole rock samples. New data also include pillow rim glass analyses from Rose  
569 atoll, whole rock data from Dino seamount, and new whole rock data on Rose and Malulu lavas.  
570 Whole rock data for the Rose atoll and the Malulu and Papatua seamounts was published by  
571 Jackson et al., 2010. All data not produced by this study was previously published and downloaded  
572 from Georoc (<http://georoc.mpch681mainz.gwdg.de/georoc>). Figure modified after Jackson et al.  
573 (2020).

574

575 **Figure S2. Age-distance relationship for Arago and Macdonald volcanoes, with projected**  
576 **ages for interloper volcanoes Moki, Malulu, Dino, Papatua, and the Rose atoll for both**  
577 **Macdonald and Arago plume origin.** Hawaiian hotspot data are shown for reference. This figure  
578 uses the great circle distances between current hotspot locations and a related volcano along the  
579 Wessel and Kroenke (2008) reconstructed trends. The volcanoes in this study plot in between the  
580 CAVL Macdonald volcanoes and the Macdonald hotspot-related Tokelau islands, suggesting that  
581 they bridge a geographic gap in Macdonald-type isotope geochemistry. Ages have been estimated  
582 for the five interloper volcanoes, based on the location of each volcano on the along-track distance  
583 trends, for both a Macdonald and Arago hotspot origin. Assuming Macdonald origin for all  
584 seamounts and the Rose atoll, Moki is ~51 Ma, Papatua is ~46 Ma, Malulu is ~44 Ma, Rose atoll is ~43 Ma, and Dino is ~39 Ma. Assuming Arago

585

586 origin, Moki is ~27 Ma, Papatua is ~25 Ma, Malulu is ~23 Ma, Rose atoll is ~22 Ma, and Dino is  
587 ~21 Ma. Age data used in this plot are provided in Jackson et al. (2020). Figure modified after  
588 Jackson et al. (2020).  
589

590 **Figure S3. Total alkali versus SiO<sub>2</sub> diagram for whole rock lavas analyzed in this**  
591 **study.** Whole rock data from other Cook-Austral volcanoes are shown for reference. The dashed  
592 line represents the boundary between the alkali (above the line) and tholeiitic (below the line)  
593 fields. The samples analyzed here plot broadly in the region defined by other volcanoes from the  
594 Cook-Austral volcanic lineament. Major elements are shown as normalized to 100% totals on a  
595 volatile-free basis. Major element data for the Malulu hyaloclastite (EX1702-12-5) are not shown,  
596 as only clinopyroxenes were analyzed.  
597

598 **Figure S4. Trace element spider diagrams for whole rock and clinopyroxene samples from**  
599 **study volcanoes.** Trace element concentrations are normalized to pyrolite from McDonough and  
600 Sun (1995). Whole rocks are shown in the top panel, and clinopyroxenes in the lower panel.  
601

## 602 **References Cited**

- 603 Beguelin, P., M. Bizimis, C. Beier, and S. Turner, 2017, Rift–plume interaction reveals multiple  
604 generations of recycled oceanic crust in Azores lavas. *Geochimica et Cosmochimica*  
605 *Acta*, v. 218, p. 132–152.  
606
- 607 Eisele, J., Abouchami, W., Galer, S.J.G., and Hofmann, A.W., 2003, The 320 kyr  
608 Pb isotope evolution of Mauna Kea lavas recorded in the HSDP-2 drill core.  
609 *Geochemistry, Geophysics, Geosystems*, v. 4, 8710, doi:10.1029/2002GC000339.  
610
- 611 Frisby, C., Bizimis, M. and Mallick, S., 2016, Hf–Nd isotope decoupling in bulk abyssal  
612 peridotites due to serpentinization. *Chemical Geology*, v. 440, p. 60-72.  
613
- 614 Gagnon, J.E., Fryer, B.J., Samson, I.M., Williams-Jones, A.E., 2008, Quantitative analysis of  
615 silicate certified reference materials by LA-ICPMS with and without an internal  
616 standard. *Journal of Analytic Atomic Spectrometry*, v. 23, p. 1529–1537.  
617
- 618 Gale, A., M. Laubier, S. Escrig, and C. H. Langmuir, 2013, Constraints on melting processes and  
619 plume-ridge interaction from comprehensive study of the FAMOUS and North Famous  
620 segments, Mid-Atlantic Ridge. *Earth and Planetary Science Letters*, v. 365, p. 209–220,  
621 doi:10.1016/801j.epsl.2013.01.022.  
622
- 623 Garçon, M., Boyet, M., Carlson, R.W., Horan, M.F., Auclair, D., and Mock, T.D., 2018, Factors  
624 influencing the precision and accuracy of Nd isotope measurements by thermal ionization  
625 mass spectrometry. *Chemical Geology*, v. 476 p. 493–514.  
626
- 627 Hart, S.R., and Blusztajn, J., 2006, Age and geochemistry of the mafic sills, ODP site 1276,  
628 Newfoundland margin. *Chemical Geology*, v. 235, p. 222–237.  
629
- 630 Jackson, M.G., Hart, S.R., Konter, J.G., Koppers, A.A.P., Staudigel, H., Kurz, M.D., Blusztajn,

631 J., and Sinton, J.M., 2010, The Samoan hotspot track on a “hotspot highway”:  
632 Implications for mantle plumes and a deep Samoan mantle source. *Geochemistry,*  
633 *Geophysics, Geosystems*, v. 11, Q12009, doi:10.1029/2010GC003232.  
634

635 Jackson, M.G., Koga, K.T., Price, A., Konter, J.G., Koppers, A.A.P., Finlayson, V.A., Konrad,  
636 K., Hauri, E.H., Kylander-Clark, A., Kelley, K.A., and Kendrick, M.A., 2015, Deeply-  
637 dredged submarine HIMU glasses from the Tuvalu Islands, Polynesia: Implications for  
638 volatile budgets of recycled oceanic crust. *Geochemistry, Geophysics, Geosystems*, v. 16,  
639 p. 3210-3234, DOI: 10.1002/2015GC005966.  
640

641 Jackson, M.G., Halldórsson, S.A., Price, A., Kurz, M.D., Konter, J.G., Koppers, A.A.P., Day,  
642 J.M.D., 2020, Contrasting old and young volcanism from Aitutaki, Cook Islands:  
643 Implications for the origins of the Cook-Austral volcanic chain. *Journal of Petrology,*  
644 *egaa037*, <https://doi.org/10.1093/petrology/egaa037>.  
645

646 Jochum, K., Stoll, B., Herwig, K., Willbold, M., Hofmann, A., Amini, M., Aarburg, S.,  
647 Abouchami, W., Hellebrand, E., Mocek, B., Raczek, I., Stracke, A., Alard, O., Bouman,  
648 C., Becker, S., Dücking, M., Brätz, H., Klemd, R., Bruin, D., Canil, D., Cornell, D.,  
649 Hoog, C.-J., Dalpe, C., Danyushevsky, L., Eisenhauer, A., Gao, Y., Snow, J., Groschopf,  
650 N., Günther, D., Latkoczy, C., Guillong, M., Hauri, E., Höfer, H., Lahaye, Y., Horz, K.,  
651 Jacob, D., Kasemann, S., Kent, A., Ludwig, T., Zack, T., Mason, P., Meixner, A., Rosner,  
652 M., Misawa, K., Nash, B., Pfänder, J., Premo, W., Sun, W., Tiepolo, M., Vannucci, R.,  
653 Vennemann, T., Wayne, D., and Woodhead, J., 2006, MPIDING reference glasses for in  
654 situ microanalysis: new reference values for element concentrations and isotope ratios.  
655 *Geochemistry, Geophysics, Geosystems*, v. 7, Q02008.  
656

657 Jochum, K., Weis, U., Schwager, B., Stoll, B., Wilson, S.A., Haug, G.H., Andreae, M.O.,  
658 Enzweiler, J., 2016, Reference values following ISO guidelines for frequently requested  
659 rock reference materials. *Geostandards and Geoanalytical Research*, v. 40, p. 333-350.  
660

661 Johnson, D.M., Hooper, P.R., and Conrey, R.M., 1999, XRF analysis of rocks and minerals for  
662 major and trace elements in a single low dilution Li-tetraborate fused bead. *Advances in*  
663 *X-Ray Analysis*, v. 41, p. 843–867.  
664

665 Knaack, C.M., Cornelius, S.B., and Hooper, P.R., 1994, Trace element Analysis of rocks and  
666 minerals by ICP-MS. Open File Report, GeoAnalytical Lab. Washington State  
667 University, p. 10.  
668

669 McDonough, W.F., Sun, S.S., 1995, The composition of the Earth. *Chemical Geology*, v. 120, p.  
670 223-253.  
671

672 Melson, W.G., O'Hearn, T., and Jarosewich, E., 2002, A data brief on the Smithsonian Abyssal  
673 Volcanic Glass Data File. *Geochemistry, Geophysics, Geosystems*, v. 3, p. 1-11,  
674 doi:10.1029/2001GC000249.  
675

676 Munker, C., Weyer, S., Scherer, E. and Mezger, K., 2001, Separation of high field strength

677 elements (Nb, Ta, Zr, Hf) and Lu from rock samples for MC-ICPMS measurements.  
678 *Geochemistry, Geophysics, Geosystems*, v. 2, p. 1064, doi:10.1029/2001GC000183.  
679

680 Oulton, J., Humayun, M., Fedkin, A., and Grossman, L., 2016, Chemical evidence for  
681 differentiation, evaporation and recondensation from silicate clasts in Gujba. *Geochimica*  
682 *et Cosmochimica Acta*, v. 177, p. 254–274.  
683

684 Price, A.A., Jackson, M.G., Blichert-Toft, J., Hall, P.S., Sinton, J.M., Kurz, M.D., and Blusztajn,  
685 J., 2014, Evidence for a broadly distributed Samoan-plume signature in the northern Lau  
686 and North Fiji Basins. *Geochemistry, Geophysics, Geosystems*, v. 15, p. 986-1008, doi:  
687 10.1002/2013GC005061.  
688

689 Price, A.A., Jackson, M.G., Blichert-Toft, J., Blusztajn, J., Conatser, C.S., Konter, J.G.,  
690 Koppers, A.A.P., and Kurz, M.D., 2016, Geochemical evidence in the Northeast Lau  
691 Basin for subduction of the Cook-Austral volcanic chain in the Tonga Trench.  
692 *Geochemistry, Geophysics, Geosystems*, v. 17, p. 1694-1724,  
693 doi:10.1002/2015GC006237.  
694

695 Reinhard, A.A., Jackson, M.G., Koornneef, J.M., Rose-Koga, E.F., Blusztajn, J., Konter, J.G.,  
696 Koga, K.T., Wallace, P.J., Harvey, J., 2018, Sr and Nd isotopic compositions of  
697 individual olivine-hosted melt inclusions from Hawai’I and Samoa: Implications for the  
698 origin of isotopic heterogeneity in melt inclusions from OIB lavas. *Chemical Geology*, v.  
699 495, p. 36-49.  
700

701 Tanaka, T., Togashi, S., Kamioka, H., Amakawa, H., Kagami, H., Hamamoto, T., Yuhara, M.,  
702 Orihashi, Y., Yoneda, S., Shimizu, H., Kunimaru, T., Takahashi, K., Yanagi, T., Nakano,  
703 T., Fujimaki, H., Shinjo, R., Asahara, Y., Tanimizu, M., and Dragusanu, C., 2000, JNdi-  
704 1: A neodymium isotopic reference in consistency with LaJolla neodymium. *Chemical*  
705 *Geology*, v. 168, p. 279–281.  
706

707 Weis, D., Kieffer, B., Maerschalk, C., Barling, J., de Jong, J., Williams, G.A., Hanano, D.,  
708 Pretorius, W., Mattielli, N., Scoates, J.A., Goolaerts, A., Friedman, R.M., Mahoney, B.J.,  
709 2006, High-precision isotopic characterization of USGS reference materials by TIMS and  
710 MC-ICP-MS. *Geochemistry, Geophysics, Geosystems*, v. 7, Q08006.  
711

712 Weis, D., Kieffer, B., Hanano, D., Silva, I.N., Barling, J., Pretorius, W., Maerschalk, C., Mattielli,  
713 N., 2007, Hf isotope compositions of U.S. Geological Survey reference materials.  
714 *Geochemistry, Geophysics, Geosystems*, v. 8, Q06006.  
715

716 Wessel, P., and Kroenke, L.W., 2008, Pacific absolute plate motion since 145Ma: an assessment  
717 of the fixed hot spot hypothesis. *Journal of Geophysical Research*, v.113, B06101.  
718 <https://doi.org/10.1029/2007JB005499>.  
719

720 White, W.M., Albarede, F. and Telouk, P., 2000, High-precision analysis of Pb isotope ratios by  
721 multi-collector ICP-MS. *Chemical Geology*, v. 167, p. 257-270.  
722

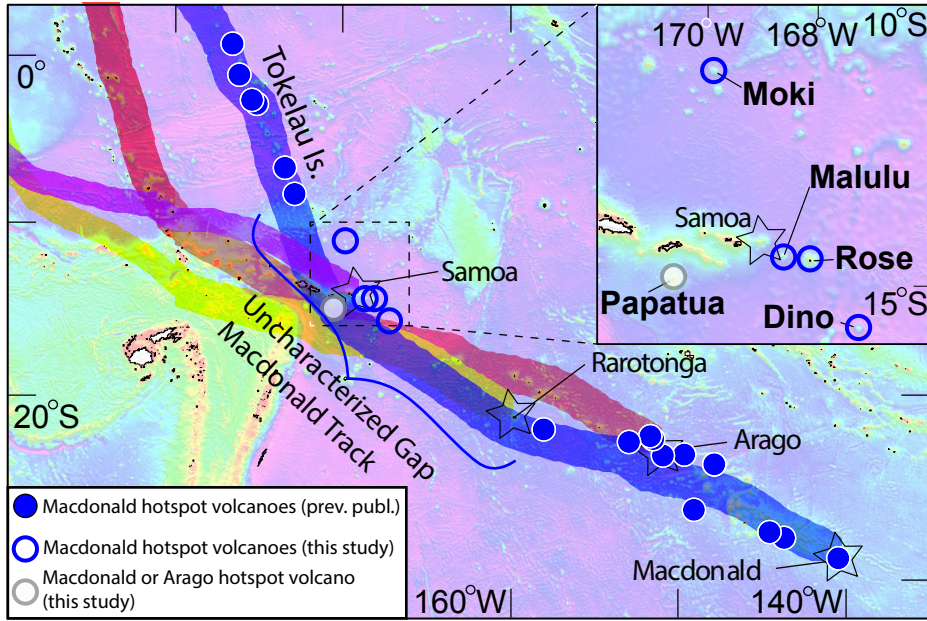


Figure 1

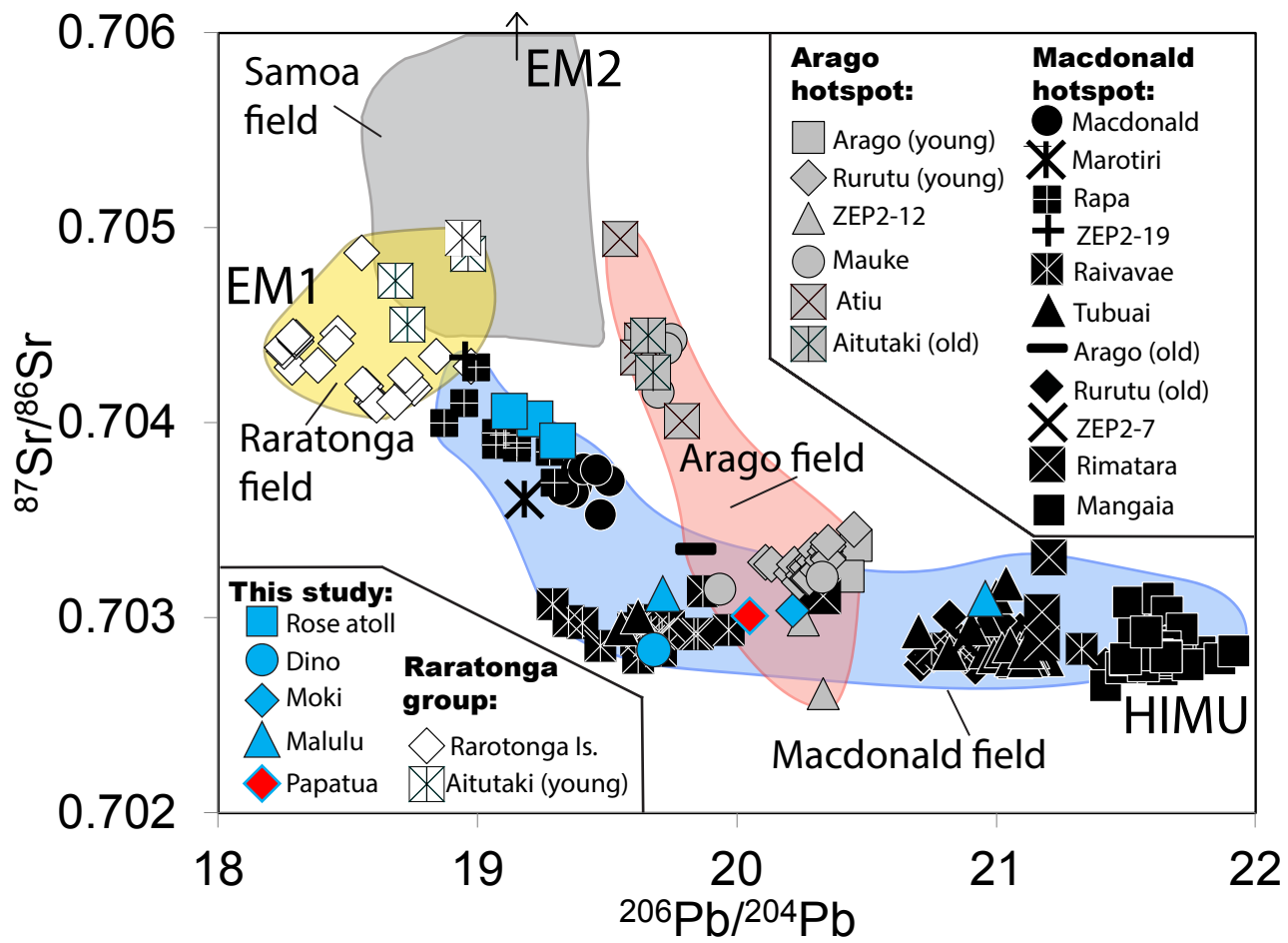


Figure 2

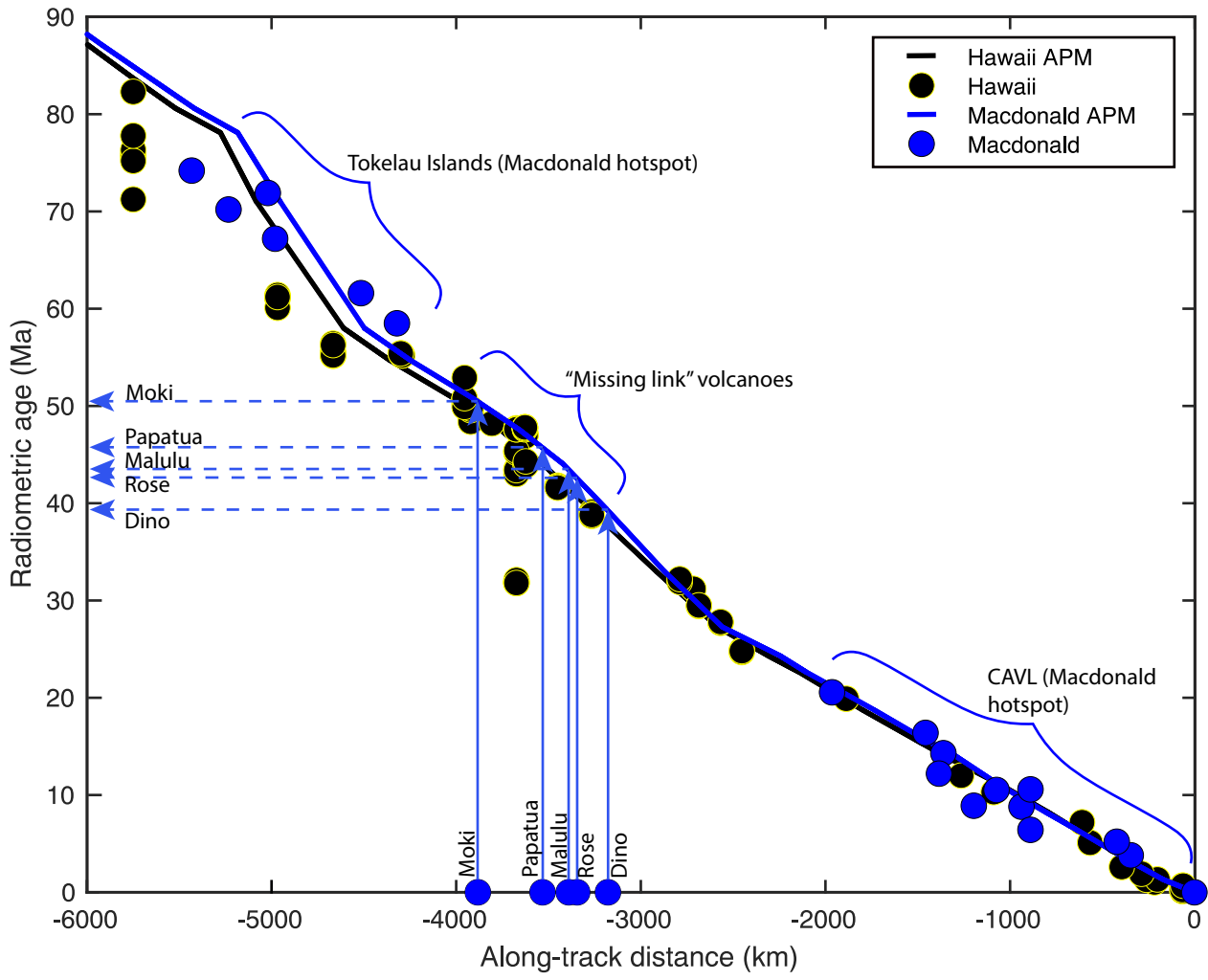


Figure 3

Table S1. Radiogenic isotopic compositions for whole rocks, glass, and clinopyroxene separates from non-Samoan "interloper" seamounts in the Samoan region.<sup>1</sup>

Sample ID	Volcano name	Material analyzed	Latitude	Longitude	<sup>87</sup> Sr/ <sup>86</sup> Sr	2SE	<sup>143</sup> Nd/ <sup>144</sup> Nd	2SE	<sup>176</sup> Hf/ <sup>177</sup> Hf	2SE	<sup>206</sup> Pb/ <sup>204</sup> Pb	2SE	<sup>207</sup> Pb/ <sup>204</sup> Pb	2SE	<sup>208</sup> Pb/ <sup>204</sup> Pb	2SE
EX1702-D7-2 <sup>2</sup>	Moki smt.	cpx	-11.1682	-169.8922	0.703037	0.000005	0.512908	0.000005	0.282922	0.000003	20.2209	0.0016	15.6205	0.0012	40.0478	0.0031
EX1702-D7-2 rep <sup>3</sup>	Moki smt.	cpx	-11.1682	-169.8922	0.703034	0.000005	0.512911	0.000004								
EX1702-D11-1 <sup>3</sup>	Smt D (Dino)	whole rock	-15.7331	-167.2646	0.702872	0.000009	0.512989	0.000005			19.6917	0.0029	15.6201	0.0025	39.2270	0.0059
EX1702-D11-1 rep <sup>4</sup>	Smt D (Dino)	whole rock	-15.7331	-167.2646	0.702795	0.000003	0.512985	0.000004			19.7050	0.0078	15.6162	0.0069	39.3336	0.0198
EX1702-D3-2 <sup>4</sup>	Rose atoll	glass	-14.5377	-168.0799	0.704014	0.000003	0.512817	0.000003			19.2401	0.0005	15.6203	0.0005	39.0252	0.0017
AVON2/3-D66-1 <sup>3</sup>	Rose atoll	whole rock	-14.6433	-168.1956	0.704085	0.000006	0.512798	0.000003			19.1025	0.0058	15.5980	0.0047	38.9144	0.0107
AVON2/3-D66-1 <sup>5</sup>	Rose atoll	whole rock	-14.6433	-168.1956	<i>0.704137</i>		<i>0.512796</i>				<i>19.14</i>		<i>15.62</i>		<i>38.98</i>	
AVON2/3-D65-18 <sup>5</sup>	Rose atoll	whole rock	-14.4890	-168.2609	<i>0.703923</i>		<i>0.512846</i>				<i>19.32</i>		<i>15.61</i>		<i>39.1615</i>	
EX1702-D12-5 <sup>2</sup>	Malulu smt	cpx	-14.4689	-168.6389	0.703121	0.000005	0.512979	0.000003	0.283051	0.000004	19.7237	0.0007	15.5812	0.0007	39.4479	0.0018
EX1702-D12-5 rep <sup>4</sup>	Malulu smt	cpx	-14.4689	-168.6389	0.703101	0.000003	0.512982	0.000002			19.7483	0.0059	15.5877	0.0056	39.4271	0.0162
AVON2/3-D67-11 <sup>3</sup>	Malulu smt	whole rock	-14.4988	-168.6631	0.703096	0.000006	0.512982	0.000003								
AVON2/3-D67-11 rep <sup>1</sup>	Malulu smt	whole rock	-14.4988	-168.6631	0.703100	0.000007	0.512982	0.000003			20.9563	0.0024	15.6535	0.0017	40.9142	0.0048
AVON2/3-D67-11 rep <sup>2</sup>	Malulu smt	whole rock	-14.4988	-168.6631	0.703108	0.000006	0.512980	0.000003								
AVON2/3-D67-11 rep <sup>3</sup>	Malulu smt	whole rock	-14.4988	-168.6631	0.703102	0.000007	0.512981	0.000003								
AVON2/3-D67-11 <sup>5</sup>	Malulu smt	whole rock	-14.4988	-168.6631	<i>0.703108</i>		<i>0.512765</i> <sup>7</sup>				<i>20.96</i>		<i>15.66</i>		<i>40.71</i>	
ALIA-DR129-05 <sup>6</sup>	Papatua smt	whole rock	-14.9705	-170.5900	<i>0.703009</i>		<i>0.512976</i>				<i>20.0614</i>		<i>15.6561</i>		<i>39.6569</i>	
BCR-2 <sup>2</sup>		powder			0.705010	0.000004	0.512623	0.000010	0.282873	0.000003	18.7561	0.0026	15.6210	0.0032	38.7311	0.0035
BCR-2 <sup>3</sup>		powder			0.705007	0.000006	0.512621	0.000002								
BCR-2 <sup>3</sup>		powder			0.705003	0.000006	0.512620	0.000002			18.7543	0.0004	15.6188	0.0004	38.7162	0.0013
BCR-2 <sup>3</sup>		powder			0.705006	0.000006	0.512625	0.000003			18.7415	0.0004	15.6093	0.0004	38.6795	0.0013
BCR-2 published (Weis et al. 2006, 2007) <sup>1</sup>		powder			0.705005	0.000010	0.512621	0.000012	0.282870	0.000008	18.7533	0.0195	15.6262	0.0040	38.7282	0.0405
AGV-2 <sup>4</sup>		powder			0.703981	0.000004	0.512776	0.000002			18.8704	0.0010	15.6215	0.0009	38.5527	0.0025
AGV-2 published (Weis et al. 2006, 2007) <sup>1</sup>		powder			0.703973	0.000009	0.512775	0.000010			18.8692	0.0063	15.6186	0.0071	38.5488	0.0135

1. All data in the table are reported relative to the following international standard values: Nd isotopes are corrected to JNdi value of 0.512099 (Garçon et al., 2018), Sr isotopic data to an NBS 987 value of 0.710240, Pb isotopic compositions are corrected to the NIST 981 values of Eisele et al. (2003) (16.9409, 15.4976, 36.7262), and Hf isotopic data are corrected to the JMC-475 of 0.282160. For the data from Weis et al (2006, 2007), Nd isotopic compositions are renormalized to a JNdi equivalent value of 0.512099 using Tanaka et al.'s (2000) La Jolla to JNdi-1 conversion, and their Pb isotopic data are renormalized to the NBS981 values from Eisele et al. (2003), and only teflon data are shown for the Hf isotopic dataset. Italicized data are previously published from Jackson et al (2010), and represent Sr, Nd, and unspiked Pb run by TIMS at WHOI (and are renormalized to the international standard values provided above). For the Weis et al (2006, 2007 data), errors are reported as 2SD of multiple analyses (all other errors in the table are 2SE), except for the BCR analysis at University of South Carolina (which is the 2SD of 5 analyses of the same BCR-2).

2. All leaching, wet chemistry (sample dissolutions and chemical separations) and mass spectrometry (all using MC-ICP-MS) for Sr, Nd, Pb and Hf isotopes completed at U. South Carolina.

3. Leaching and wet chemistry (sample dissolutions and chemical separations) for Sr, Nd, and Pb completed at UCSB. Sr and Nd mass spectrometry completed on UCSB TIMS, and Pb mass spectrometry (if any) completed on U. South Carolina MC-ICP-MS.

4. Leaching and wet chemistry (sample dissolutions and chemical separations) for Sr, Nd, and Pb completed at UCSB. Sr and Nd mass spectrometry completed on UCSB TIMS, and Pb mass spectrometry (if any) completed on WHOI MC-ICP-MS.

5. Leaching and wet chemistry (sample dissolutions and chemical separations) and mass spectrometry for Sr, Nd, and Pb completed on WHOI TIMS (data published in Jackson et al., 2010).

6. Leaching and wet chemistry (sample dissolutions and chemical separations) and mass spectrometry for Sr, Nd, and Pb completed on WHOI MC-ICP-MS (data published in Jackson et al., 2010).

7. This result is superseded by new analyses of this sample made at UCSB (also presented in this table).

Table S2. Major and trace element concentrations lavas published in this study together with prior analyses of related seamounts.

Seamount or atoll	Moki smt. <sup>1</sup>	Moki smt. <sup>2</sup>	Papua smt. <sup>3</sup>	Malulu smt. <sup>3</sup>	Malulu smt. <sup>2</sup>	Smt. D (Dino) <sup>1</sup>	Rose atoll <sup>3</sup>	Rose atoll <sup>3</sup>	Rose atoll <sup>1</sup>	Rose atoll <sup>4</sup>	Ref material <sup>1</sup>	Ref material <sup>1</sup>	Ref material <sup>2</sup>	Ref material <sup>2</sup>	Ref material <sup>4</sup>	Ref material <sup>4</sup>
Sample ID	EX1702-D7-2	EX1702-D7-2	ALIA-DR129-05	AVON2/3-67-11	EX1702-D2-5	EX1702-D11-1	AVON2/3-65-18	AVON2/3-66-1	EX1702-D3-2	EX1702-D3-2	BCR-2	BCR-2	BHVO-1	BHVO-1	ALV-519-4-1	ALV-519-4-1
Sample Info	whole rock	cpx	whole rock	whole rock	cpx	whole rock	whole rock	whole rock	whole rock	glass	(this study)	(publ)	(this study)	(publ)	(this study)	(publ)
<b>XRF or ICP-MS Solution Majors</b>																
SiO <sub>2</sub>	36.30		38.65	41.77		45.00	45.97	46.18	46.43	51.57	54.30	54.93		50.17	48.98	48.94
TiO <sub>2</sub>	4.736		3.43	3.20		1.820	3.11	1.90	2.440	2.43	2.29	2.30		2.76	0.73	0.75
Al <sub>2</sub> O <sub>3</sub>	12.34		15.67	11.63		15.52	13.26	8.89	13.85	14.61	13.54	13.71		13.80	16.44	16.53
FeO*	11.37		10.84	13.56		8.88	11.45	11.53	11.83	9.54	12.47	12.61		11.17	8.91	9.03
MnO	0.125		0.18	0.22		0.061	0.17	0.18	0.154	0.14	0.20	0.20		0.17	0.17	0.17
MgO	6.59		3.33	7.09		2.43	8.46	19.18	6.43	6.13	3.60	3.66		7.27	9.71	9.41
CaO	15.15		10.66	15.64		12.60	11.22	9.17	11.30	10.16	7.15	7.24		11.52	12.48	12.58
Na <sub>2</sub> O	1.17		3.14	1.95		3.01	2.03	1.47	2.89	3.05	3.18	3.17		2.33	2.10	2.07
K <sub>2</sub> O	0.83		1.96	1.11		2.42	1.50	0.58	0.54	0.91	1.80	1.80		0.53	0.08	0.1
P <sub>2</sub> O <sub>5</sub>	2.586		3.26	1.50		0.594	0.27	0.24	0.893	0.39	0.35	0.37		0.28	0.07	0.09
Total (majors only)	91.18		91.13	97.67		92.43	97.44	99.32	96.77	98.92	98.86			99.66	99.52	99.52
LOI	8.11		8.87	2.33		7.27	2.56	0.68								
Sum of Majors and LOI	99.29		100.00	100.00		99.69	100.00	100.00	99.55							
<b>XRF or ICP-MS Solution or Laser Traces</b>																
Ni	86			120		28	148	692	144	84	12	13			189	178
Cr	456	1922	3	608	1430	34	437	1116	726	160	11	16		292	288	413
V	366	208	224	319	139	196	278	182	240	230	410	418		321	314	244
Ga	18	7.5	17	16	11.1	17	17	18	22	23	22	21		21	14	
Cu	92	1.5	54	148	1.9	117	78	54	68	57	18	20		130	137	108
Zn	218	15	174	144	25	99	151	116	158	144	130	130		106	105	83
Sc	36					43			26		33	1				
Ba	220					90			155		687	684				
Nb	82					13			24		13	12				
Rb	18					32			9		47	46				
Sr	279					266			462		338	337				
Zr	266					128			187		178	187				
Y	59					32			31		36	1				
La	75					13			23		25	25				
Ce	113					26			50		55	53				
Nd	55					19			32		29	28				
<b>ICP-MS Solution or Laser Traces</b>																
Li		0.47			1.54					8.21			4.76	4.68	4.22	4.20
Mo		0.03			0.11								1.07	1.06		
Sn		0.06			0.20								1.79	2.09		
W		bdl			0.02								0.20	0.21		
Co		24.8			21.6					37.3			43.6	44.9	51.2	48.7
Cs	0.52	bdl	1.54	0.96	0.00	0.76	0.38	0.31	0.20	0.59	1.14	1.16	0.09	0.10	0.02	0.02
Rb	17.4	bdl	37.2	28.7	0.15	30.1	21.2	12.4	7.18	25.5	46.5	46.0	8.24	9.52	2.13	2.01
Ba	219	0.72	292	257.4	2.93	90.7	65.9	103.0	151	202	683	684	128	134	24.4	24.3
Th	6.24	0.05	5.74	6.40	0.34	1.14	3.58	1.82	3.06	2.88	6.23	5.83	1.22	1.23	0.26	0.28
U	2.89	0.01	1.89	1.73	0.04	0.42	0.29	0.41	0.79	0.91	1.71	1.68	0.41	0.42	0.09	0.09
Nb	84.7	0.87	60.7	77.8	3.02	13.1	33.2	19.2	24.5	27.3	11.6	12.4	20.1	18.5	4.02	4.49
Ta	5.51	0.11	3.85	4.51	0.43	0.90	2.35	1.32	1.67	1.66	0.78	0.79	1.17	1.17	0.24	0.27
La	74.3	3.02	88.1	76.1	9.32	12.9	26.2	15.8	24.6	22.2	25.7	25.1	15.4	15.4	2.68	2.81
Ce	114	10.2	101.0	145.9	29.7	26.6	68.0	35.8	49.6	50.8	53.5	53.1	37.5	38.1	6.75	6.90
Pb	2.39	0.02	3.59	3.40	0.11	0.89	2.94	1.91	2.40	2.69	10.4	10.6	2.02	2.04	0.21	0.27
Pr	14.3	1.69	15.1	18.1	5.02	3.91	8.16	4.50	6.54	6.19	6.97	6.83	4.93	5.42	0.94	1.02
Nd	56.3	9.16	61.4	77.7	27.9	17.6	37.0	20.8	28.9	28.2	29.2	28.3	24.4	24.8	4.86	5.17
Sr	290	55.2	822	1066	164	272	145	244	477	458	346	337	390	399	64	71
Zr	280	52.6	271	278	214	130	208	132	194	195	184	187	171	175	34.5	39.9
Hf	7.03	2.47	6.21	5.97	6.95	3.29	5.71	3.46	5.05	4.49	5.03	4.97	4.26	4.44	0.95	1.11
Sm	10.7	2.51	12.24	17.65	7.43	4.69	9.51	5.47	7.29	6.82	6.94	6.55	5.91	6.17	1.62	1.66
Eu	3.38	0.83	3.93	5.68	2.37	1.76	3.06	1.80	2.48	2.19	2.13	1.99	2.03	2.05	0.63	0.65
Gd	9.83	2.48	12.51	15.40	6.79	5.70	8.69	4.99	7.19	6.36	7.11	6.81	6.20	6.29	2.28	2.58
Tb	1.39	0.38	1.89	2.11	0.91	0.95	1.31	0.75	1.09	0.86	1.18	1.08	0.94	0.95	0.42	0.48
Dy	8.05	1.77	11.72	10.79	4.14	5.96	6.93	4.16	6.15	5.14	6.99	6.42	4.90	5.27	3.24	3.44
Ho	1.58	0.31	2.71	1.83	0.65	1.26	1.20	0.74	1.12	0.90	1.46	1.31	0.94	0.98	0.71	0.79
Y	60.9	8.0	129.5	54.0	18.0	32.1	31.6	18.5	31.5	22.8	36.2	36.1	26.2	26.2	18.6	22.3
Er	3.96	0.72	7.66	4.06	1.37	3.40	2.81	1.71	2.72	2.31	3.81	3.67	2.44	2.50	2.21	2.33
Tm	0.53	0.09	1.09	0.50	0.16	0.47	0.35	0.22	0.37	0.30	0.55	0.53	0.34	0.33	0.33	0.33
Yb	3.22	0.51	6.89	2.71	0.90	2.88	1.90	1.26	2.10	1.79	3.34	3.39	1.93	1.99	2.30	2.43
Lu	0.51	0.07	1.19	0.39	0.12	0.46	0.28	0.18	0.31	0.24	0.51	0.50	0.27	0.28	0.34	0.39
Sc	35.9	80.8	14.6	28.6	79.8	44.6	29.0	24.9	26.4	23.9	33.4	33.5	31.9	31.4	42.6	43.0

1. For whole rock samples EX1702-D7-2, EX1702-D11-1, and EX1702-D3-2, major elements and a subset of trace elements analyzed by XRF, and some of these trace elements and an additional set of trace elements were analyzed by solution ICP-MS. A BCR-2 reference material was analyzed as an unknown together with the samples in this study and previously published data on the BCR-2 are reported in [Jochum et al. \(2016\)](#) and shown in this table for reference.

2. Trace elements and a subset of major elements on clinopyroxene separates (EX1702-D7-2 and EX1702-D12-5) were run by solution ICP-MS at the University of South Carolina. Published major and trace element concentrations for this reference materials are from [Jochum et al. \(2016\)](#) and are shown in this table for reference; the major element concentrations from [Jochum et al. \(2016\)](#) are here normalized to 100% total with all Fe reported as FeO.

3. Italicized data were previously published in [Jackson et al. \(2010\)](#), and include two lavas from Rose atoll: 1 lava from Papua seamount, and 1 lava from Malulu seamount. LOI's (Loss On Ignition) are estimated for these 4 lavas after [Jackson et al. \(2010\)](#).

4. The major element composition of the EX1702-D3-2 glass is the average of three different spot analyses by electron probe. The major element composition of the ALV-519-4-1 reference glass is the average of 22 different spot analyses analyzed during the same analytical session as EX1702-D3-2, and the data are shown together with published of ALV-519-2 values from [Melson et al. \(2002\)](#). The trace element composition of the EX1702-D3-2 glass is the average of four different spot analyses by LA-ICP-MS. The trace element composition of the ALV-519-4-1 reference glass is the average of 8 different spot analyses during the same analytical session as EX1702-D3-2, and the data are shown together with published data on ALV-519-4-1 from [Gale et al. \(2013\)](#) and compiled in [Jackson et al. \(2015\)](#).

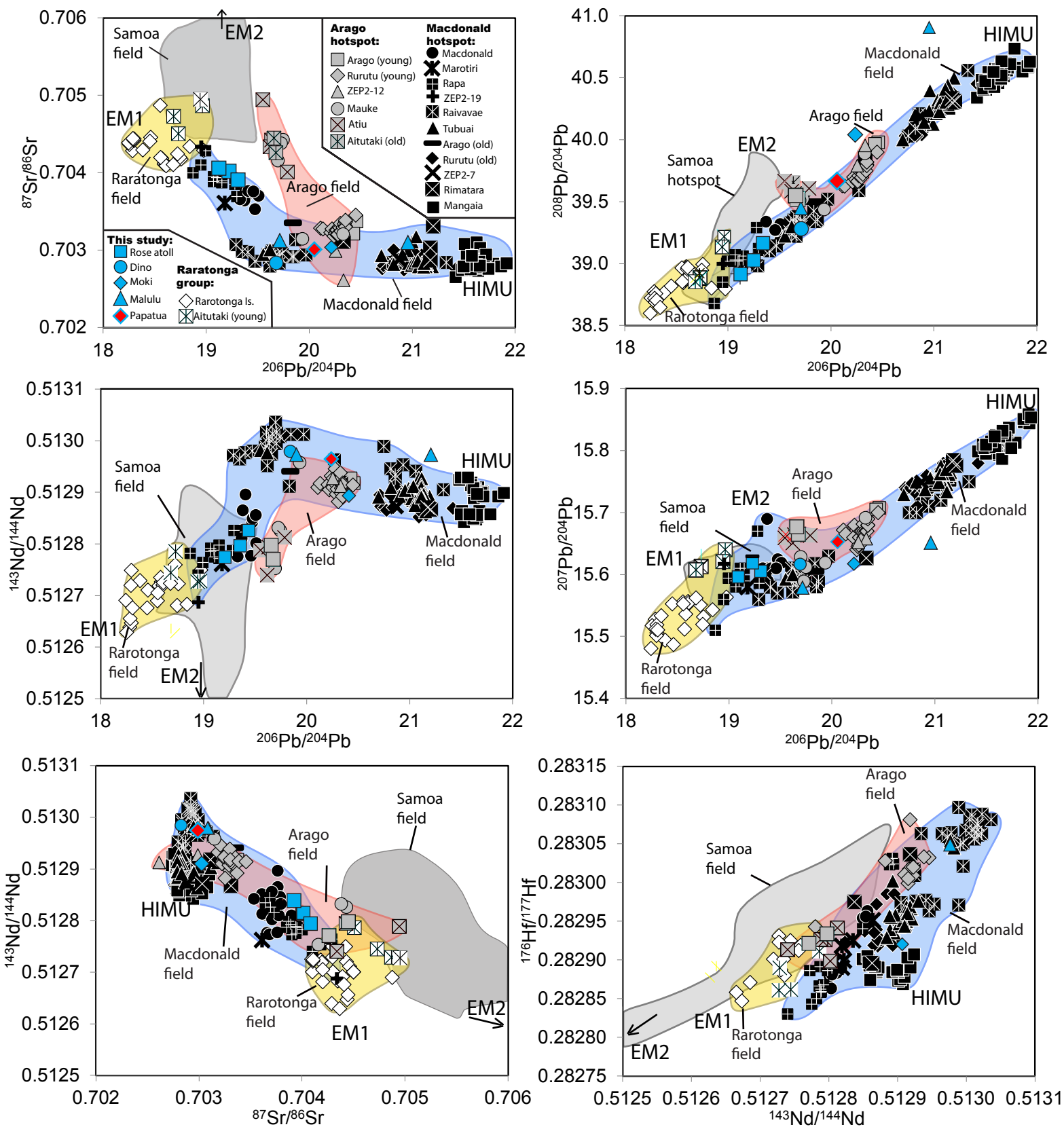


Figure S1

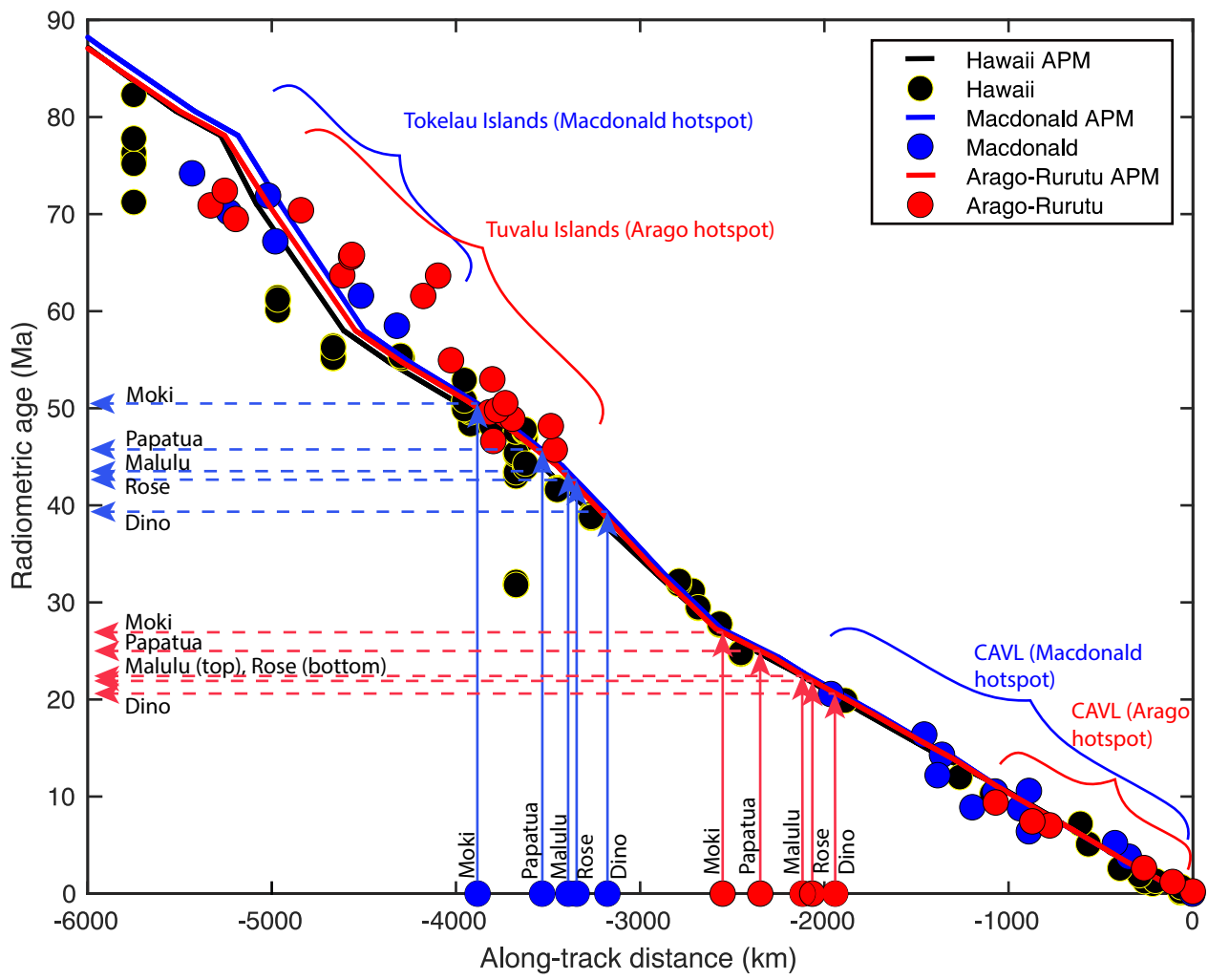


Figure S2

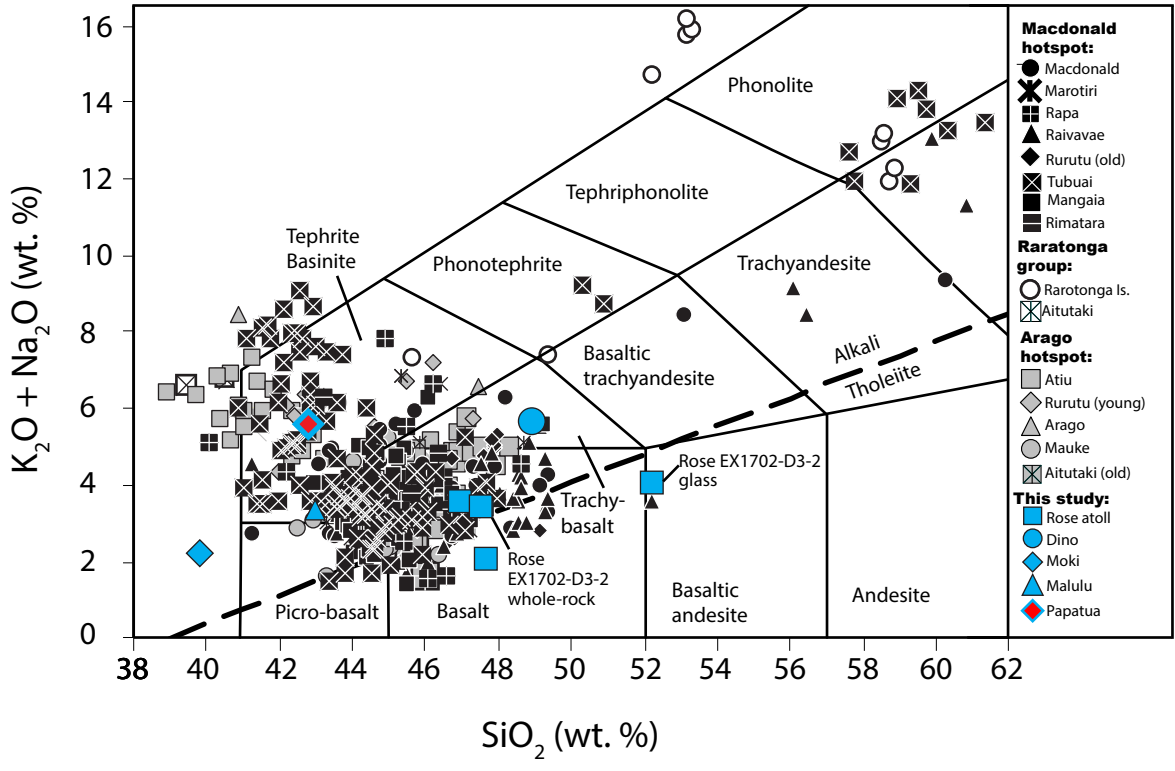


Figure S3

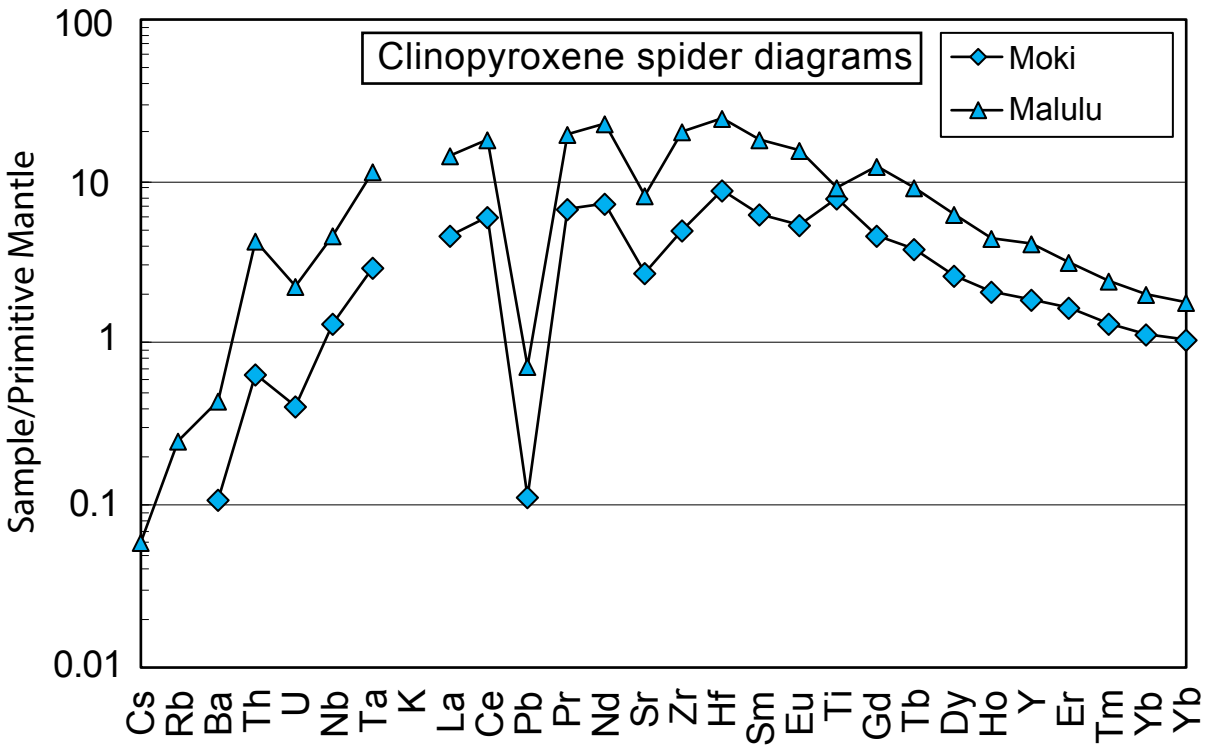
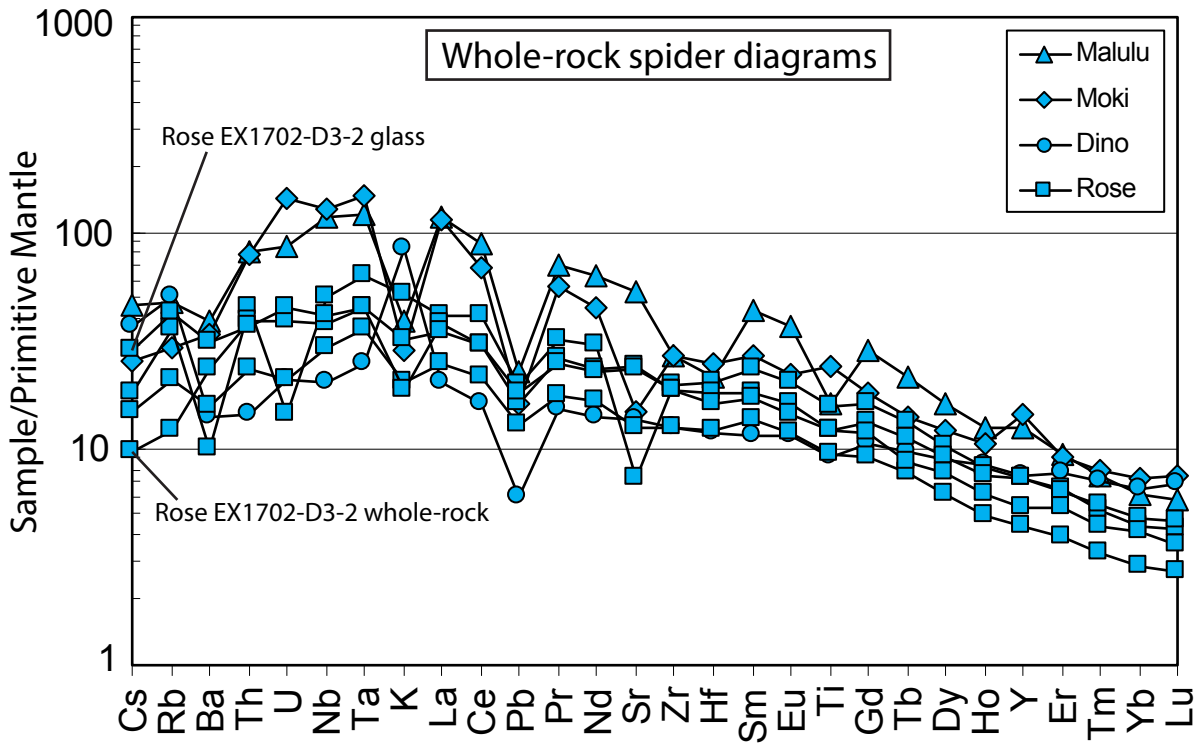


Figure S4